Department of Physics and Astronomy, University of Canterbury, Private Bag 4800, Christchurch, New Zealand

The Effect of Annealing on the Optical Properties of Zinc Oxide

by

Alex Neiman

A thesis submitted in
fulfillment of the
requirements for the Degree of
Master of Science
in Physics

Supervisors: Prof. R. Reeves, Dr. M Allen
University of Canterbury
2014

Abstract

Photoluminescence spectroscopy of bulk zinc oxide under different annealing conditions was examined. The effect of the annealing atmosphere, temperature and time on the optical properties of zinc oxide were studied to investigate the influence on the intrinsic defects present. The wafers used were bulk $+c$ ZnO grown by Tokyo Denpa using the hydrothermal technique. The annealing effect on both zinc and oxygen faces was investigated. The dominant donor bound exciton related to aluminum, labelled in the literature as I_6 demonstrated a splitting of 0.3 meV. The origin of this splitting has been linked to an interaction between aluminum and hydrogen, through its reaction to atmospheric dependent annealing. The removal of the hydrothermal hydrogen peak at 3.3624 eV has uncovered some fine structure. After Arrhenius analysis of this fine structure it was shown it is excited states of bound excitons. This fine structure has been loosely associated with vibrational and rotational excited states. The behaviour of all the optical features present in the photoluminescent spectra under annealing has a relation with the carrier concentration of the samples.

Contents

List of Figures

Chapter 1

Introduction

1.1 ZnO

For the past 30 years zinc oxide (ZnO) has been the subject of interest due to its optical properties that offer potential in electronics. ZnO has a wide direct band gap of 3.3 eV at room temperature shown in figure 1.1 (a). Due to the wide band gap ZnO is visible blind and absorbs in the ultraviolet (UV) region of the electromagnetic spectrum. ZnO is visible blind as photons of lower energy than the band gap are not absorbed making it transparent. These properties mean that ZnO could be used in multi-layered solar cells as it could sit above smaller bandgap materials collecting UV light and letting lower energy photons through to be absorbed below it, increasing the efficiency of solar cells. The multi-layered solar cells are more efficient as the energy lost by the photons is less, as each layer absorbs photons of only slightly higher energy or of the energy of the bandgap. The wide direct band gap makes ZnO a candidate for use in blue/UV/white LEDs or laser diodes. The direct nature of the band gap means that opto electronic devices created from ZnO will be efficient indicating it could replace the commonly used direct band gap materials of a similar width. This replacement is desired as the generally used blue or white LEDs (GaN or InGaN) use rarer, more expensive, elements that have no current recycling infrastructure. The band structure shown in figure 1.1 (a) is simplified showing the singular complication of multiple valence bands. The three valence

bands are a result of the crystal field and spin-orbit coupling. ZnO is also non-toxic as demonstrated by its common use in sunscreens.

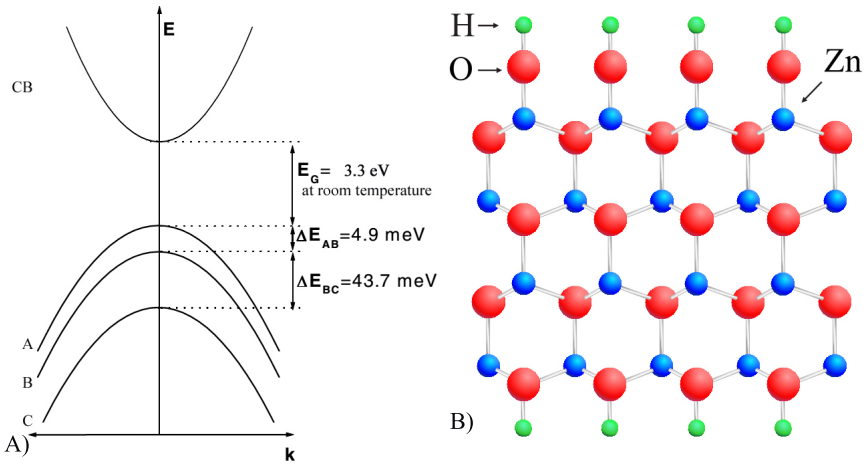

Figure 1.1: a) Simple band structure of ZnO showing bandgap and three valence bands b) Bulk ZnO in hexagonal wurtzite structure, with hydroxyl and hydrogen stabilisation on the polar surfaces.

Bulk ZnO crystallizes in a hexagonal wurtzite structure, where each zinc (Zn) atom is at the centre of a tetrahedron of oxygen (O) atoms. Figure 1.1 (b) shows a cross section of the structure of ZnO with the vertical direction being the c axis. The surface of the planes across the c axis (horizontal in figure 1.1 (b)) are not intrinsically stable [3]. The c planes of ZnO are thought to be stabilised by hydroxyl termination [4]. The plane across the c axis terminating with a single Zn atom bonded to a hydroxal group has been labelled as the Zn face. Similarly the plane across the c axis terminating with a O atom bonded to three Zn atoms and a hydrogen atom is labelled the O face. The $+c$ axis is the label for ZnO that has been grown off the Zn face of ZnO, alternatively the $-c$ axi s is the label for ZnO grown off the O face of ZnO. The O face is the dominant surface seen in molecular beam epitaxy and pulsed laser deposition growth methods. Wafers cut from the $+c$ plane of bulk ZnO crystal were investigated within this thesis due to the unique polarity differences and discrimination of features [2]. In this thesis the wafers, from which the individual samples were cut, were bulk double sided polished $+c$ ZnO. The wafers were hydrothermally grown by TEW Tokyo Denpa Co Ltd.

Figure 1.2 (a) shows a schematic diagram of the hydrothermal growth technique used by Tokyo Denpa [1]. The ZnO material is dissolved in a solution of LiOH and KOH in a section of a Pt lined autoclave. The autoclave is platinum lined to stop the LiOH and KOH mineralisers from reacting with the walls of the autoclave. The solution moves by convection into the upper growth region of the chamber where the seed crystals are held. The nature of the seed crystals determine the axis of growth, $+c$ or $-c$. Figure 1.2 (b) shows the different planes that are studied in ZnO. The O and Zn polar planes found on the $+c$ have been investigated to greater extent than the other planes of ZnO.

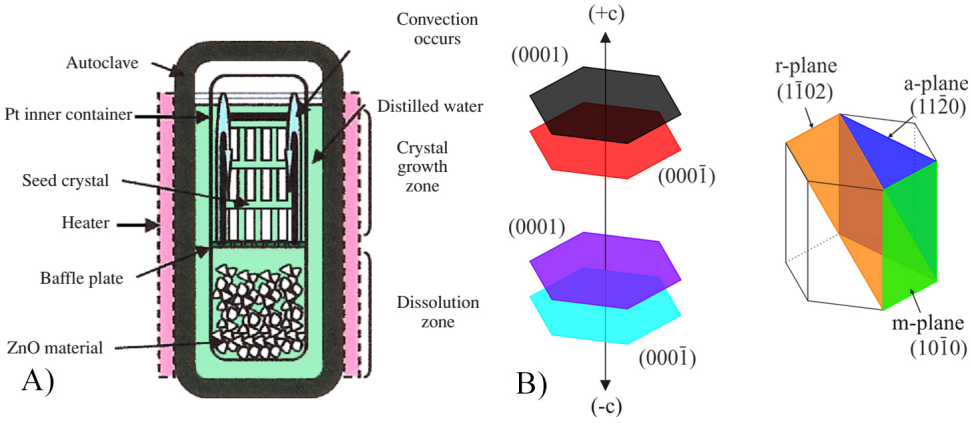

Figure 1.2: a) Schematic of the hydrothermal growth system [1]. b) Planes of ZnO [2].

ZnO is radiation hard [5]. It does not interact with high energy electrons, gamma radiation or neutron bombardment. While ZnO is radiation hard it is known to react in a few distinct cases. Low energy electrons (2 MeV) have been shown to form vacancies [6] and high density electron beams have been used to anneal bulk crystals [7]. As ZnO is radiation hard it could be used as a material for components in hazardous environments without shielding, such as space or in super colliders.

One of the major advantages of ZnO over similar band gap semiconductors is the high exciton dissociation energy of 60 meV. The bound electron-hole pair that is

correlated by the Coulomb effect is an exciton. The dissociation energy of an exciton is the energy required to isolate it to its constituents of a free electron and a free hole. The high dissociation energy of excitons in ZnO means that they still exist at room temperature as they are not thermally dissociated. At 300 K a thermal energy of $k_{\mathrm{B}}T = 26$ meV is still considerably less than the exciton dissociation energy of 60 meV. This is a major advantage as photoluminescence is enhanced by the formation of excitons within a crystal causing light emitting devices to be more efficient. Exitons enhance photoluminescence as it guarantees that the wavefunctions of the combining electron and hole overlap. This also leads to less chance of non radiative relaxation of the constituents of the recombining pair. Exciton based devices have increased speed and efficiency [8]. Real crystals are never perfectly ordered and this creates opportunities for excitons to become bound to defects (vacancies and dislocations) and impurities (substitutional and interstitial). As will be discussed in section 1.3.1 the dominant PL from ZnO at low temperature is from the recombination of excitons bound to neutral donors.

The native defects in ZnO causes the crystal to be n-type and no study that is reproducible has found a reliable way to grow p-type ZnO, severely reducing the current use of ZnO. The nature of the native defects that cause the n-type conductivity is still under investigation. Initially this was attributed to oxygen vacancies ($\mathrm{V_O}$) [9]. $\mathrm{V_O}$ are unlikely to be the cause as the free carrier concentrations have been shown to be much larger than the concentration of $\mathrm{V_O}$ [10]. Hydrogen has been proposed as a candidate for the cause of the n-type conductivity prevalent in bulk ZnO [11].

There are four known elements that are thought to be shallow donors within ZnO. They are hydrogen, aluminium (Al), gallium (Ga) and indium (In). The elements Al, Ga and In which are group III elements are thought replace the Zn ion in the lattice to form donors. In photoluminescence literature the emission from the

donor bound exciton complexes that form are labelled I_4, I_6, I_8 and I_9 respectively [12].

Even with this extended period of research into ZnO there are still a lot of unknowns particularly the behaviour of hydrogen. In many semiconductors hydrogen behaves counter to the prevailing conductivity i.e. an acceptor in n-type and a donor in p-type semiconductors [13]. This is not the case in ZnO which is naturally n-type and hydrogen behaves as a donor [14]. In oxide semiconductors there is evidence that hydrogen passivates acceptors [15]. The behaviour of hydrogen in ZnO and its importance can be investigated using the high mobility and reactivity of hydrogen. In a recent paper by Matsubara et al [16] it has been shown from first principles calculations that hydrogen attracts the other donor impurities, that it would be expected to repel and forms complexes leading to deep donor levels.

1.2 Annealing of ZnO

Annealing is the process of heating a material in a controlled fashion. Annealing, by thermal activation, increases the mobility of the constituents of the crystal giving the possibility for the structure to rearrange and react with the atmosphere. Annealing of crystalline semiconductors has been reported to improve the structure of the crystal by giving mobility to the constituents allowing a more ordered structure to form [17, 18]. The increase in mobility can also remove impurities through out gassing or be used to drive dopants into the crystal. These processes can be achieved by control of prior annealing treatment, annealing atmosphere and annealing temperature.

Annealing is a technique that is generally used for a single specific goal. In this thesis the effect of annealing on ZnO will be studied. Annealing is used after ion implantation where it is used to repair the damage from the process. In addition to doping, ion implantation can help to understand native defects when the specific crystal constituent atoms are implanted. Native defects such as antisites, interstitials and vacancies are all possible results of implantation. The effect of annealing on unaltered bulk ZnO has not fully been studied and this limits the understanding that ion implantation can give. There are three basic factors that effect annealing : the atmosphere, the temperature and the time. In this thesis all three factors were investigated.

The composition of the atmosphere during annealing can drastically change the outcome of the procedure. Annealing of ZnO in forming gas (NH_3) produces visible pits on the surface and drives hydrogen into the crystal, whereas annealing in O_2 removes hydrogen and improves the crystal quality. By annealing in an inert atmosphere (nitrogen (N)) , a reactive atmosphere (oxygen (O_2)) and comparing it to the bulk crystal the behaviour of the reactive reagents in ZnO can be identified.

The temperature of annealing effects what is out gassed or driven in. The temperature that materials are annealed at is the most understood part of annealing. When investigating the recovery of a material through annealing a temperature series of broad steps is carried out with a single favourable outcome out gassing of an element, crystalline quality or driving in a dopant. The study carried out in this thesis tried to find threshold temperature at which out gassing of different elements occur and how quality improves as a function of temperature. This was done by doing a small annealing step size starting at a low temperature.

The time taken in annealing is generally a fixed time dictated by the initial annealing time a research group used. In this thesis the effect of the annealing time is looked at by using a single sample and analysing it at a series of intervals during an extended anneal.

Two annealing techniques were used in this thesis due to the large range of temperatures investigated.

1.3 Photoluminescence Spectroscopy

Photoluminescence spectroscopy (PL), a powerful non-destructive investigation technique, is the analysis tool that is used throughout this thesis. PL can be used to directly probe the electronic structure of a semiconductor within the band gap as the observed emission is a direct result of that structure. Different radiative process in semiconductors can have similar emission energies meaning that correlating the emission with the band structure within the band gap and then to the nature of semiconductor is not straight forward.

PL in the most basic terms, is the experimental technique where photons illuminate a material and the resulting light emission is examined. In PL spectroscopy there are multiple variations that can be used: temperature dependent spectroscopy, magneto-spectroscopy, electric potential dependent spectroscopy, power dependent spectroscopy, polarisation dependent spectroscopy, time resolved spectroscopy and excitation wavelength dependent spectroscopy also known as photoluminescent excitation (PLE). In this thesis temperature dependent spectroscopy is used as a technique to assist in emission peak identification.

At low temperature < 10K, emission efficiency is maximised and more luminescent features from the sample can be seen. The emission is maximised as at low temperature non-radiative vibration, rotational and phonon modes within the lattice are reduced to a minimum. The emission of centres at low temperatures have less energy variation from thermal broadening giving smaller line widths, increasing discrimination of features. Additionally, more features are seen at low temperatures as emission from bound sources is possible. Elevated temperatures provide sufficient thermal energy to release the bound state and thus shut down that particular emission centre. At raised temperatures quasi particles like excitons can also be dissociated.

Temperature dependent spectroscopy is a technique where the intensity and wavelength of emission as a function of temperature is investigated. Bound excitons within semiconductors are freed from their bound states as the temperature of the material increases. Consequently the intensity of the PL line decreases with temperature. However, before the quenching of the line occurs it is possible to see increases in intensity of the excited states of bound excitons with small increases in temperature. The temperature dependence of PL that has such thermal activation energies is known to follow a model based on the Arrhenius equation [19]. An analytically derived formula for this behaviour is

$$I(T) = I(0)\frac{1 + \sum_{q=1}^{w} D_q e^{\frac{-E_q}{k_B T}}}{1 + \sum_{j=1}^{m} C_j e^{\frac{-E_j}{k_B T}}} \tag{1.1}$$

where $I(T)$ is the integrated intensity of the feature at a given temperature T, $I(0)$ is the intensity at 0 K, w is the number of negative thermal quenching mechanisms, m is the number of thermal quenching mechanisms, E_q is the activation energy of the negative thermal quenching mechanism, E_j is the activation energy of the thermal quenching mechanism, k_B is Boltzmann constant and C_j and D_q are weighting factors [19]. Extraction of the PL intensity from the temperature dependent data can be used to find the excitation energy of the excited states to uncover their origins.

1.3.1 Photoluminescence of ZnO

When a photon above the band gap is incident on a semiconductor the most probable outcome is for it to be absorbed, creating an electron excited into the conduction band and a hole in the valence band. Emission can then result in a number of ways such as:

- Direct recombination of the hole and electron which is a band to band transition.
- Recombination of a neutral donor with a free hole, hD^0.

- Recombination of a free electron with a neutral acceptor, eA^0.

In ZnO the majority of the emission comes from excitons where the electron and hole combine through the Coulomb interaction and create a bound state. The excitonic state is slightly lower in energy than a free hole and free electron in their respective valence and conduction bands.

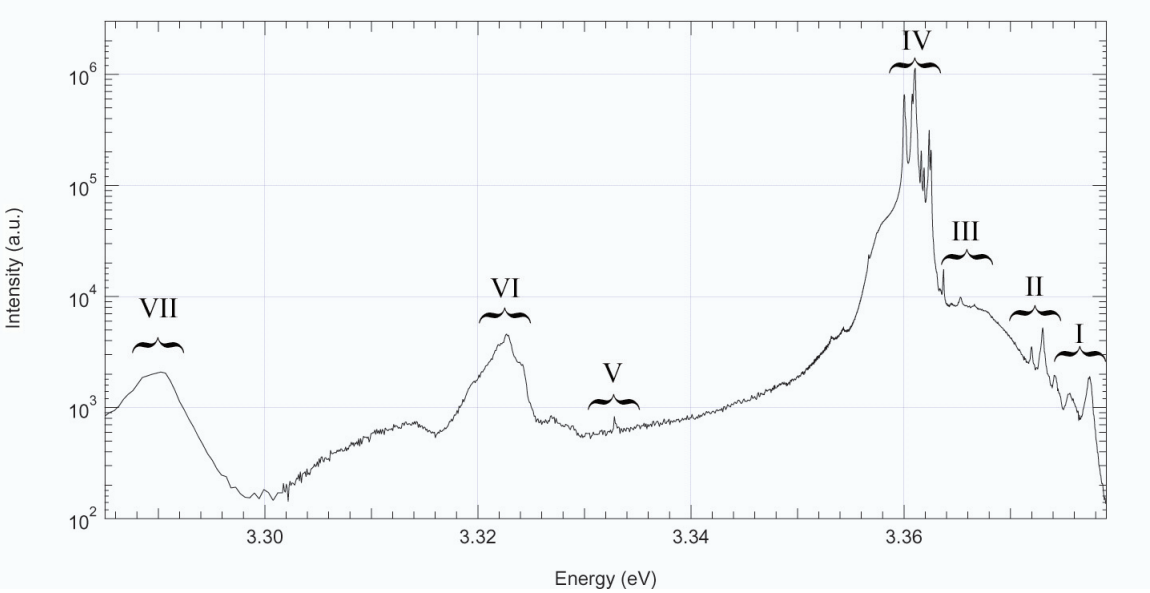

Figure 1.3: The near band edge luminescence of hydrothermal ZnO at 3.9 K with the excitons labelled I) free excitons, II) ionised replicas, III) B excitons, IV) donor bound exciton, V) Y line, VI) two-electron satellite and VII) phonon replica. An explanation of these terms is provided in the text.

The spectrum in figure 1.3 is the typical 3.9 K spectrum of a Zn face bulk $+c$ as received sample from Tokyo Denpa. As received samples have been labelled as reference samples in order to compare treatment processes. In figure 1.3 the labels show regions where the described excitons are usually found. Not all possible types of excitons are shown.

In ZnO the free exciton is split into longitudinal and transverse excitons that are defined by how they propagate through the lattice [20]. In this model an exciton propagates by recombining to form a photon which excites the lattice to create an

exciton at another location. Figure 1.3 I indicates the location of these two excitons in luminescence. In the literature they are labelled A_T and A_L with the longitudinal exciton having the higher energy. The free excitons have been identified by there emission energy which is red-shifted from the band gap by the dissociation energy of 60 meV.

It has become apparent in the above disccussion about excitons that multiple different energy shifts need to be mentioned to describe a exciton. For clarity common energy shifts will be defined throughout the thesis as:

- The dissociation energy - the energy required to isolate an exciton in to its constituents of a free electron and a free hole.
- The localisation energy - the energy shift between the free excitons and a bound exciton.
- The ionisation energy - the energy required to ionise a donor or acceptor.

Figure 1.3 IV shows the neutral donor bound exciton region. A neutral donor bound exciton is an electron-hole pair that is bound to a neutral donor within the lattice. The radiative recombination creates a photon that is red-shifted by the localisation energy from the PL energy of the free exciton. In the literature they are labelled D^0X.

Figure 1.3 VII shows the region of the first phonon replica of the neutral donor bound excitons. Phonon replicas are the red shifted emission of the bound exciton where a phonon is generated as the exciton collapses. In polar materials at low temperature Frölich coupling is responsible for the exciton-longitudinal optical phonon interaction. This coupling is dominant in ZnO and is the result of the Coulomb interaction between the exciton and the longitudinal electric field of longitudinal phonons [21]. Thus the phonon peak is red shifted by the longitudinal optical phonon energy.

Figure 1.3 VI shows the region of the two-electron satellites for the D^0X peaks. In a two-electron satellite transition some energy from the bound exciton recombination promotes the donor electron to the n= 2 state from its ground level. Consequently the photon is red shifted from the D^0X parent by the n= 2 $\rightarrow$ 1 energy gap. Splitting in the two-electron satellites has also been seen and is due to the different excited states available for the electron of the defect i.e. where an electron could be excited into the 2s or 2p states [12].

Figure 1.3 II shows transitions from ionised donor bound excitons where the exciton is bound to the ionised state of the donor. Ionised defect bound excitons can be identified using magneto-spectroscopy [22]. The current method for finding the defect that is being ionised is making correlations between the intensity ratios of features present [22]. Ionised defect bound excitons would exhibit an increase in intensity as a function of slight temperature increase as the ionised state could be thermally excited. This means temperature dependent spectroscopy could be used to identify these emission sources as they would exhibit negative thermal quenching.

B excitons are where an exciton has its hole located in the B valence band. This blue shifts the emission by 4.9 meV which is the splitting between A$\rightarrow$ B valence bands. Region III in figure 1.3 shows the location of the neutral donor bound B excitons. The structure of this region mirrors the previously discussed neutral donor bound excitons as the B excitons are bound to the same neutral donors. As the hole for the B excitons is in an excited state, temperature dependent PL would show these features exhibiting negative thermal quenching. B excitons of all features are theoretically possible.

Figure 1.3 V shows the position of the Y-lines. The Y-lines have been attributed to the emission from an extended defect bound exciton complex. One possible cause of the Y-lines is a defect consisting of two ionised donors separated by a distance

greater than the Bohr radius of the effective mass of the donor. The excited state of the Y line is two electrons bound strongly to the defect donors with antiparallel spin and a hole weakly bound to the resulting complex. The ground state of the Y-line is a single electron being bound to the defect donors. The Y-lines as shown from cathodoluminescence are localised around line defects [23]. Increase in the Y-line intensities in PL are indicative of reducing crystalline quality as they are linked to structural defects within the crystal.

The spectrum in figure 1.3 does not include all possible emission sources. Some of the sources not included are excitons bound to acceptors, donor-acceptor pair transitions and vibrational and rotational excited states.

Neutral acceptor bound excitons have a theoretically higher localisation energy than neutral donor bound excitons and lie between the two electron satellite region and the neutral donor bound excitons [22]. Neutral acceptor bound excitons are an electron-hole pair that are bound to a neutral acceptor and the radiative recombination creates a photon red-shifted from the recombination emission of a free exciton. Neutral acceptor bound excitons are labelled A^0X in the literature but no experimentally verified stable acceptors are known for ZnO. Nitrogen, lithium and sodium are theoretically acceptors in ZnO [12].

Donor-acceptor pair transitions have a high localisation energy as both the donor and acceptor levels lie within the bandgap thus red shifting the emission from the free excitons. In ZnO they are thought to be located in the region $2.8-3.2$ eV around the end of the phonon replicas but before the broad visible feature of the defect band.

Vibrational and rotational excited states have been found using photoluminescence excitation (PLE) for neutral donor bound features [24]. PLE is an experimental technique where the wavelength of excitation is varied to excite features directly.

Estimations of vibrational and rotational excited states of bound features can be found by drawing an analogy to molecular vibrations. A model using the Kratzer potential

$$V(r) = -2D\left(\frac{a}{r} - \frac{a^2}{2r^2}\right) \tag{1.2}$$

has been developed. The energy difference between the ground and excited states of the bound defect is found by analytically solving the radial Schrödinger equation [25]. The expression for this energy difference is

$$E(\nu, J) = \frac{-(2ma^2/\hbar^2)D^2}{\left[\left(\nu + \frac{1}{2}\right) + \sqrt{\left(J + \frac{1}{2}\right)^2 + \left(\frac{2ma^2}{\hbar^2}\right)D}\right]^2} \tag{1.3}$$

where ν is the vibrational quantum number, J is the rotational quantum number, D is the localisation energy, m is the band mass, a is the equilibrium internuclear separation. With the values for ZnO being $m = 0.7m_0$ and $a = 0.8$ nm taken from Meyer et al [24]. These states should also be visible in high resolution PL. High resolution PL is required as the splitting between excited states is of the order of 2 meV. As they are excited states they should exhibit negative thermal quenching in temperature dependent PL.

Chapter 2

Experimental Procedure

2.1 Annealing

A three element furnace was used for high temperature annealing at or above 300°C. The sample was placed in the middle of the hot furnace and the temperature gradient was set such that there was a constant known temperature at the sample. Each element of the furnace was monitored by a thermocouple. The atmosphere was controlled by constantly pumping the desired gas into the end of the tube, giving a constant flow over the surface of the samples. A flow rate of 80 standard cubic centimeters per minute (sccm) was used. The samples were removed from the furnace with care to reduce the thermal damage that could occur during rapid cooling.

Low temperature annealing below 300°C was carried out in an oven. The atmosphere during annealing was controlled by placing the samples in a purpose blown glass capsule within the oven and the desired gas pumped through from an external gas bottle. The capsule was split into two separated halves to allow the sample to be inserted and removed. The flow into the capsule was 1.5 liters per minute as losses from the capsule were unknown. A high flow rate was used in this setup to insure a known atmosphere. Due to the awkward nature of the set-up there was little control over the cooling of the samples.

2.2 Photoluminescence

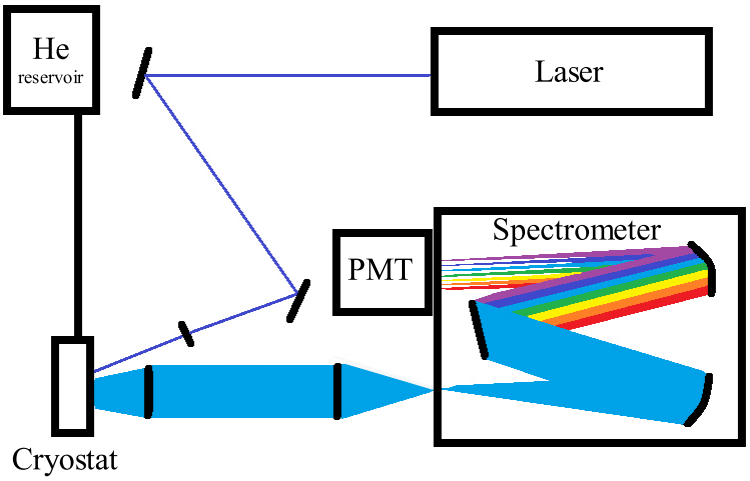

Figure 2.1: Experimental photoluminescence set-up.

The experimental set-up for PL is shown in figure 2.1. Predominantly a 25 mW Kimmon (IK series) helium cadmium (HeCd) 325 nm metal-vapour laser was used as the above bandgap excitation source. A secondary excitation source was used while the HeCd laser was being refurbished. This secondary source was a Spectra-Physics argon laser optimised on the 333.6 nm line. When the HeCd laser was used a specialised notch filter was placed directly after the laser to reduce plasma lines. When the argon laser was used a UV prism was placed in the beam path to reduce plasma lines. After the removal of the plasma lines the excitation source was focused on to the sample. A UV optimised lens was used to collect and collimate the emission from the excited sample. The collimated emission was then focused into a Horiba Jobin Yvon 1 m spectrometer. The focused light passed through a sharp edge long-pass filter (328 nm). To disperse the emission a 1200 line holographic grating was installed in the spectrometer.

The entrance and exit slits on the spectrometer were changed when optimising for the two different spectral regions examined. A larger slit size was used for the defect region as the intensity is significantly reduced in comparison to the near band

edge. The loss in resolution with the large slits is balanced by the broad nature of the features in the defect region. The slit widths were 8 μm for the near band edge and 50 μm for the defect band. The dispersed emission was detected using a cooled Hamamatsu (type $R943-02$) photo-multiplier tube (PMT). The PMT was cooled by a Peltier device to $-30°$C. Individual voltage pulses from incident photons were analysed in a University of Canterbury Department of Physics and Astronomy built discriminator and counter electronic system. The intensity was integrated over a second to improve the signal to noise ratio.

To maintain the low temperatures required for efficient emission the samples were placed inside a Oxford Instruments (Optistat CF2) liquid He cryostat. An inbuilt heater allowed for temperature control using an Oxford Instruments (mercuryiTC) temperature controller from 3.9 K to 300 K. All standard measurements were carried out at 3.9 K.

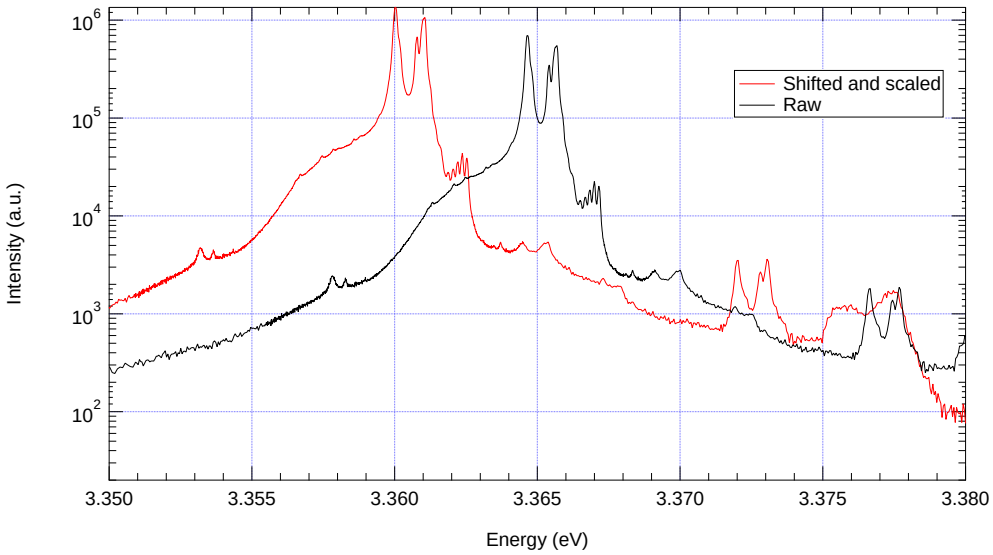

Figure 2.2: Demonstrating difference between calibrated spectra and raw spectra.

Figure 2.2 gives an example of the difference between treated spectra near band edge. In this thesis comparison of samples after treatment is critical. To facilitate this a reference sample was always mounted and analysed to correct for day to day

variation. The intensity of the near band edge spectra is scaled by a multiplication factor to the reference sample, the spectrum intensity to the right of the free excitons is used as the point of alignment. The emission in this region of the graph would only fluctuate due to the background emission during that spectrum and the optimisation of the optics. By scaling to the reference sample qualitative results can be found.

There is a slight drift in the recorded wavelength of the emission throughout measurement so all near band edge spectra are shifted to I_9 at 3.3567 eV as it is present in all spectra. This drift is due to temperature variations and mechanical fluctuations in the spectrometer. The intensity of the defect band spectra are scaled to their respective near band edge spectra at the first phonon replica. The defect band is shifted to the doubled laser line. The doubled laser line is an artifact of the diffraction grating as the dispersion of the second order is indistinguishable from doubled wavelength.

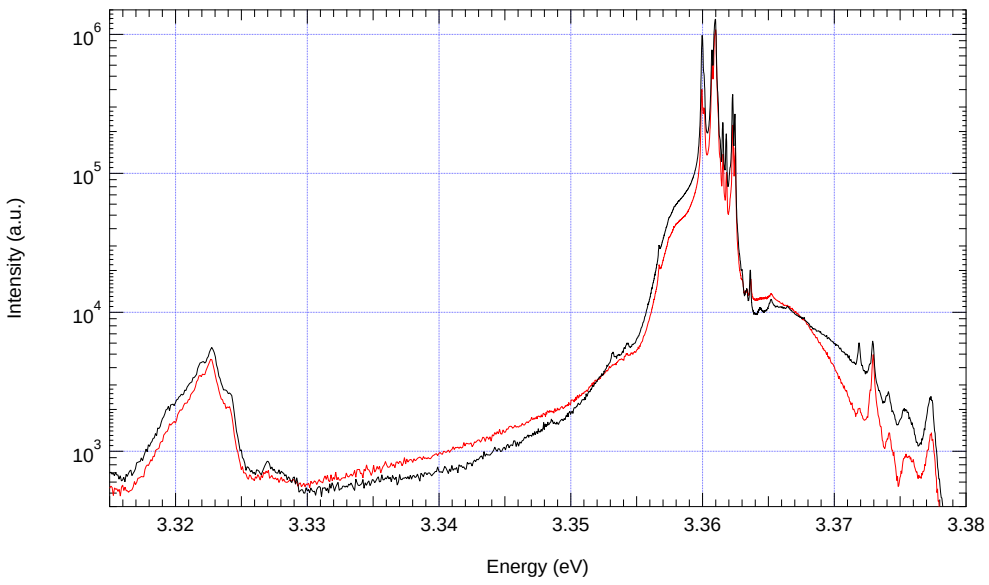

Figure 2.3: Reproducibility of near band edge spectra of hydrothermal ZnO at 3.9 K.

Figure 2.3 show the reproducibility of the PL setup, where the two spectra are from two different spots on a single reference sample. The broad feature between

the free excitons and the donor bound excitons, the intensity ratio of the neutral donor bound excitons, the ionised donor region and the features to the right of I_9 all experience a small dependence on the location of the laser spot.

Chapter 3

Atmosphere dependent annealing

The atmosphere for annealing a material is generally an inert gas or elemental component of the structure. In this thesis the effect of the annealing atmosphere is looked at by comparing an inert gas that is not a component of ZnO, N_2, and a relatively reactive gas that is a constituent of ZnO, O_2. Both these elements have previously been used as the annealing atmosphere of ZnO. In J. W. Shin et al [17] the effect of O_2 and N_2 as the annealing atmospheres on thin films of ZnO was investigated to determine how to improve the crystalline structure. Both O_2 and N_2 improve the quality of the thin films, with O_2 being more effective at improving the structure and surface quality. In J. K. Dangbégnon et al [18] the effect of the different atmospheres on the diffusion of an impurity (arsenic) into ZnO was studied. An O_2 annealing atmosphere was shown to give a more pronounced effect as shown by an increase in the emission thought to be due to an arsenic centre.

In this work annealing on both the O and Zn faces of $+c$ ZnO was performed, for 90 minutes at 600°C with a flow rate of 80 sccm for both atmospheres in the tube furnace. The samples use in this experiment were double sided polished bulk single crystals, having both an O and Zn face. To discriminate between the faces, samples were designated for use as either Zn face or O face. The samples were then annealed with the designated face facing upward in the furnace to ensure the annealing atmosphere was applied consistently. The designated face was the only face

to be investigated in PL. The PL analysis of the samples was done using excitation from the HeCd laser. A Zn face from the same wafer was used as the reference in the PL study.

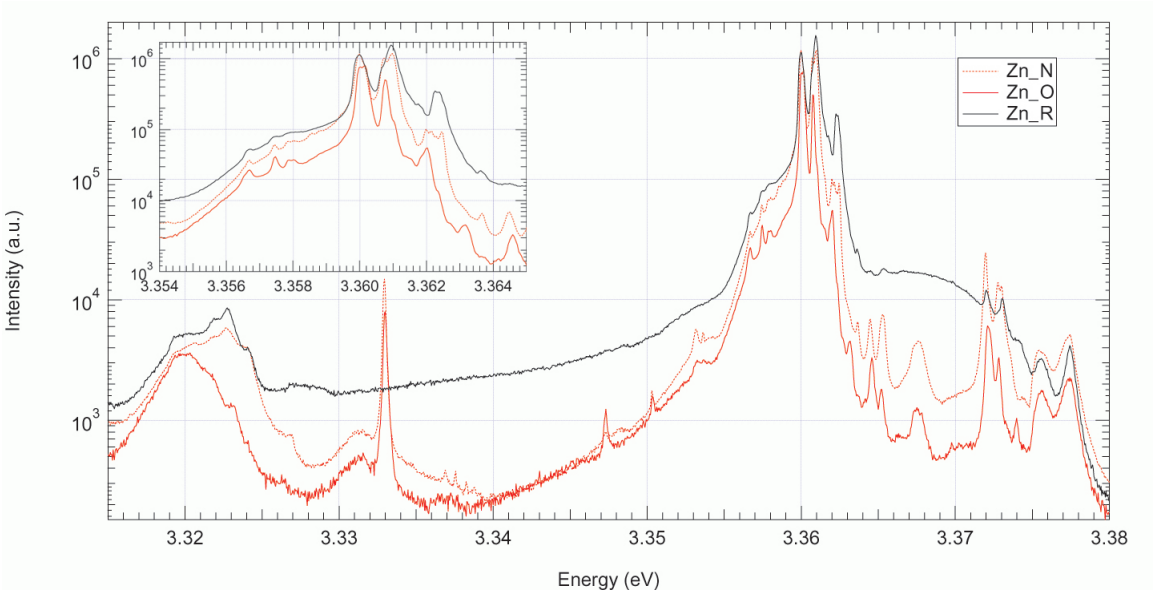

Figure 3.1: Annealing atmosphere dependent PL of the near band edge emission of the Zn face of hydrothermal ZnO at 3.9 K.

The spectra in figure 3.1 show the effect of different annealing atmospheres on the Zn polar $+c$ face of ZnO. Zn_R is the spectra of the unaltered reference sample from the same wafer. Zn_N is the spectra of the Zn face after being annealed in an N_2 atmosphere. Zn_O is the spectra of the Zn face after being annealed in an O_2 atmosphere.

The Y line at 3.333 eV is present in both annealing atmospheres showing that annealing temperature and annealing time have a greater overall effect on the structure of the crystal than the annealing atmosphere. As the Y line is an extended structural defect, structural flaws within the crystal have been exaggerated.

The neutral donor bound exciton complex at 3.3624 eV that is thought to be related to an interaction between hydrogen and the hydrothermally grown lattice is

out gassed in both N_2 and O_2 annealing atmospheres. This peak is thought to be related to H in the lattice as the neutral donor bound exciton complex introduced by H known as I_4 in the literature in melt grown ZnO, exhibits equivalent behaviour [2]. The energy shift between the two H complexes could be explained by different bonding of the H with the lattice induced by the growth conditions being distinct.

The neutral donor bound peaks $3.3550 - 3.3630$ eV show different behaviour in the two annealing atmospheres. The splitting seen in the neutral donor bound exciton peaks has not previously been reported, and has been uncovered here by the recent improvements to equipment at the University of Canterbury increasing the resolution of the spectra.

The split peak at 3.3608 eV previously described in the literature as I_6 and attributed to an aluminium (Al) complex centre shows pronouncedly different behaviour in the two different annealing atmospheres. Previous studies have shown the peak to be a single entity related to Al, suggesting the splitting is caused by complex centres that Al forms with another defect in the crystal lattice.

The O_2 atmosphere reduces one of the splitting peaks completely while it remains untouched by the N_2 atmosphere. O_2 has been shown to facilitate diffusion of defects in ZnO [18]. The peak reduction observed here supports the theory that an O_2 atmosphere increases the mobility of defects into or out of the crystal. O_2 is more reactive then N_2, suggesting that the complex centre requires the more reactive atmosphere to cause the removal of the centre.

The nature of this splitting can be further examined by looking at work done in parallel at the University of Canterbury by Robert Heinhold [2]. The splitting being caused by a complex involving H is supported by his experiments that showed the splitting peak can be reformed with annealing in forming gas. Forming gas is H rich

and facilitates the introduction of H into the lattice. This theory is supported by the increased interaction between H and O over H and N which aid the observations shown in figure 3.1.

The splitting is not present in low lithium hydrothermally grown ZnO. This does not disclude the presence of lithium (Li) being involved in the splitting centre as the hydrothermal hydrogen related peak is also absent. Annealing of the low Li samples in forming gas makes the splitting present. Hydrothermally grown low Li ZnO is achieved by high temperature annealing to migrate the high mobility Li to the surface of the bulk crystal. The crystal is then ground back to remove the volume of crystal containing the majority of Li [26]. This preparation means that under annealing the remaining Li could migrate to the surface supporting Li involvement. An annealing temperature of 600°C may not be sufficient to migrate significant concentrations of Li to the surface. When hydrogen is implanted by ion bombardment into low Li samples the splitting is present along with I_4 meaning that Li is not needed for the splitting to occur as the implantation would not cause migration of Li to the surface. The cause of the splitting of the Al complex centre is most probably due to a relationship with hydrogen in the lattice.

The effect of the atmospheres on the Al related neutral donor bound exciton complex at 3.3608 eV is visible in other regions of the spectrum. The ionised donor bound excitons in the region 3.3710 to 3.3750 eV show the same relationship meaning the H interacting with the Al does not change the shift caused by the ionisation of the Al complex. The B excitons centred at 3.3645 eV exhibit twin behaviour as well verifying that the splitting is due a variation of the donor centre that the exciton is bound to. The two electron satellite further demonstrates the effect of the annealing atmosphere on the complex binding centre.

The removal of the hydrothermal hydrogen donor bound exciton complex at 3.3624 eV uncovers a multitude of fine features at 3.3624 eV. PL is an additive technique, meaning the detected emission creating the spectra is a combination of the intensities of all radiative processes at each wavelength. Indications of the fine structures are not present in the hydrothermal hydrogen peak suggesting that the presence of hydrothermal hydrogen passivates this fine structure. This collection of emission was found to higher discrimination under time dependent annealing and these features will be further discussed in a later chapter.

At 3.3677 eV on the Zn face in both O_2 and N_2 atmospheres a peak of an unknown nature emerges. The energy separation between the neutral donor bound excitons and this peak is too large for it to be a B exciton. Temperature dependent PL or magneto-PL could identify whether the peak is an excited state. Similarities between its line shape and the neutral donor bound excitons could be drawn.

The spectra shown in figure 3.1 demonstrate that the background emission throughout the whole near band edge region is reduced by annealing.

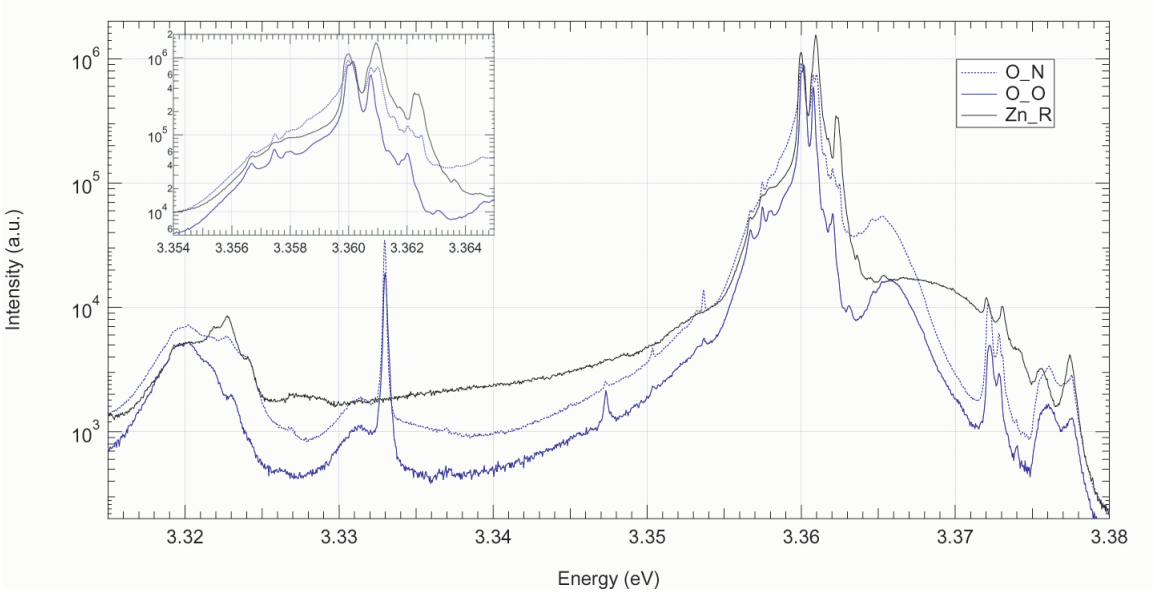

Figure 3.2: Annealing atmosphere dependent PL of the near band edge emission of the O face of hydrothermal ZnO at 3.9 K.

The spectra in figure 3.2 show the effect of different annealing atmospheres on the O polar face of $+c$ ZnO. Zn_R is the spectra of the unaltered reference sample from the same wafer. O_N is the spectra of the O face after being annealed in an N_2 atmosphere. O_O is the spectra of the O face after being annealed in an O_2 atmosphere.

The broad feature present in the region $3.3640-3.3740$ eV demonstrates a greater reduction in an O_2 annealing atmosphere on both faces of ZnO investigated. The nature of the broad feature is unknown and it demonstrates different behaviour with a polarity difference along the c axis. This feature will be further discussed in the temperature dependent annealing section as more information will be presented there. The remainder of the O face is similarly effected by annealing in the two different atmospheres as the Zn face.

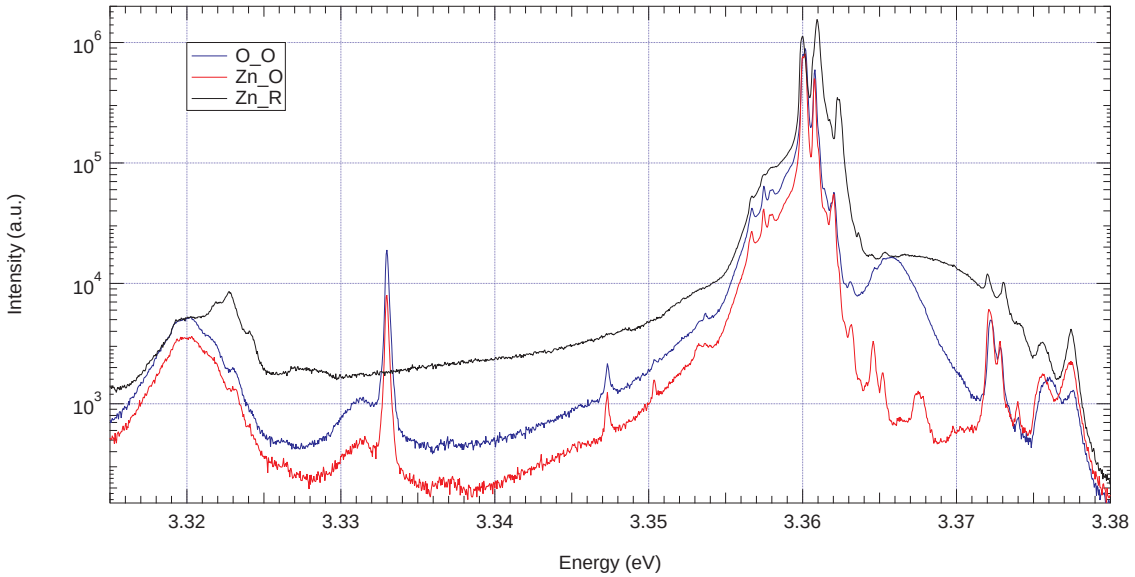

Figure 3.3: The effect of a oxygen annealing atmosphere on the surface polarity in hydrothermal ZnO at 3.9 K.

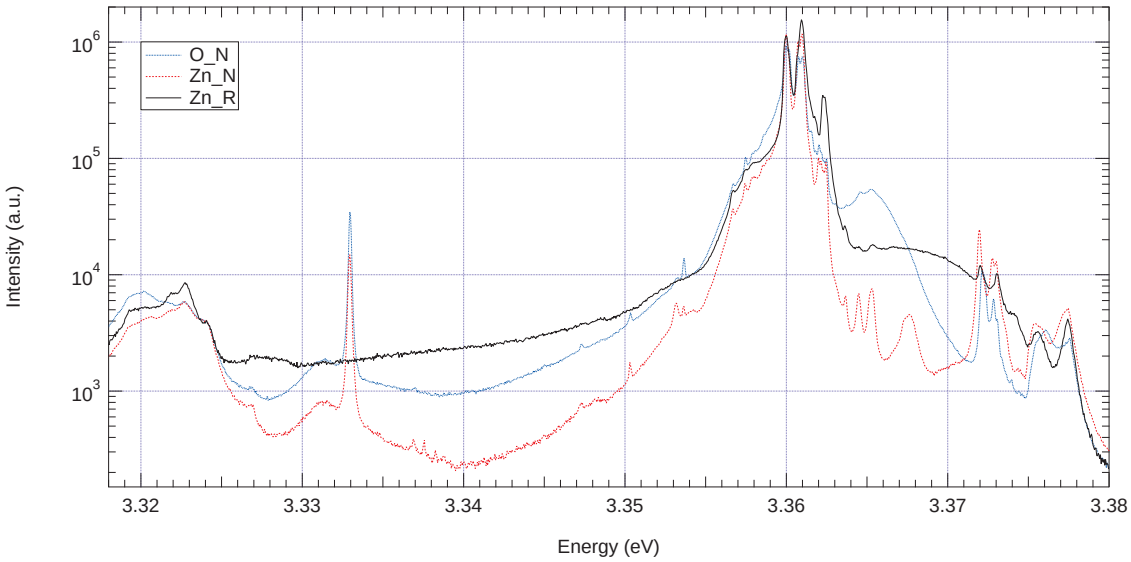

Figure 3.4: The effect of a nitrogen annealing atmosphere on the surface polarity in hydrothermal ZnO at 3.9 K.

The spectra in figure 3.3 and figure 3.4 show the effect of a O_2 and N_2 annealing atmospheres respectively on the polar Zn and O $+c$ faces of ZnO. Zn_R is the spectra of the unaltered reference sample from the same wafer in both samples. O_O is the spectra of the O face after being annealed in a O_2 atmosphere. Zn_O is the spectra of the Zn face after being annealed in a O_2 atmosphere. O_N is the spectra of the O face after being annealed in a N_2 atmosphere. Zn_N is the spectra of the Zn face after being annealed in a N_2 atmosphere.

The polarity difference remains in the annealed samples as shown in figures 3.3 and in figure 3.4. The polarity difference of the shape of the free excitons and broad feature between $3.3640 - 3.3670$ eV remain unchanged with annealing in different atmospheres.

On both faces in both annealing atmospheres there is a multitude of small peaks that arise in the region $3.3590 - 3.3350$ eV. The nature of these peaks are slightly different in the two faces in relation to the polarity of the sample. While the nature of these peaks is mostly unknown there is an argument that they could be acceptors that are no longer passivated by H. This argument is possible as theoretically ac-

ceptors have a higher localisation energy than donors, and thus would have neutral acceptor bound exciton transitions slightly red-shifted to the donor equivalents. To further support this theory H has been reported to passivate acceptors and in an O_2 annealing atmosphere these peaks have a notably higher intensity which could be correlated to the removal of the Al-H complex. To investigate this argument the donor-acceptor pair region should be investigated which was done with temperature dependent annealing.

Chapter 4

Temperature dependent annealing

The temperature of annealing is usually investigated in annealing studies looking for the temperature at which the crystalline quality, integrated PL intensity or another particular feature is optimised without respect to the other features. In this study the temperature steps started at a relatively low temperature of 100°C. Six samples were investigated in this experiment, three Zn face and three O face. The samples used in this experiment and chapter 5 are from a different wafer than chapter 3. One separate sample of each face was set aside as a reference. Two samples, again one of each face, were initially annealed at a temperature of 100°C and the final two samples were initially annealed at a temperature of 150°C. The near band edge and defect band of each sample was then measured by PL. These samples were then annealed at increasing temperature in steps of 100°C characterised at each step using PL to maximum temperatures of 700°C and 750°C respectively. An annealing atmosphere of O_2 was chosen as it effects the samples to a greater degree and therefore more thermal behaviour could be investigated. A annealing time of 30 minutes was chosen as the out gassing of H was of interest. In this study two different excitation sources were used for the reference spectra. At 100°C and 150°C annealing temperatures the HeCd laser was used, for all other spectra the argon laser was used. The resolution of the spectra was reduced as discussed later in this section. As a result the discrepancies between the two wafers used cannot be addressed until the time dependent annealing results in chapter 5 are discussed as the resolution is recovered

during that experiment.

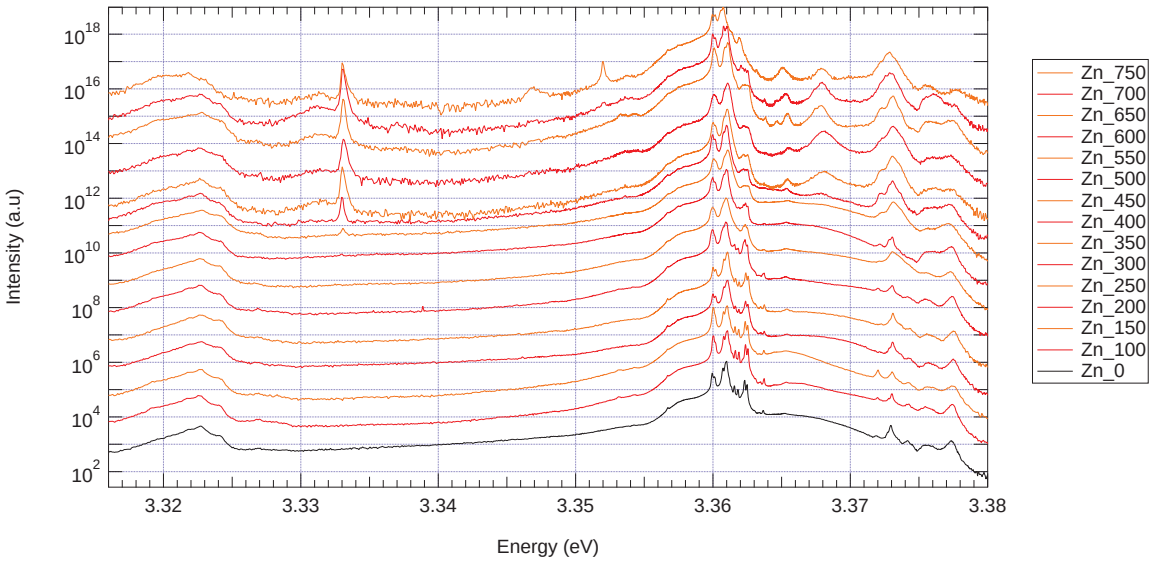

Figure 4.1: Annealing temperature dependent of the near band edge emission of the Zn face of hydrothermal ZnO at 3.9 K. Zn_100 is the Zn face annealed for 90 minutes at 100°C in an O_2 atmosphere.

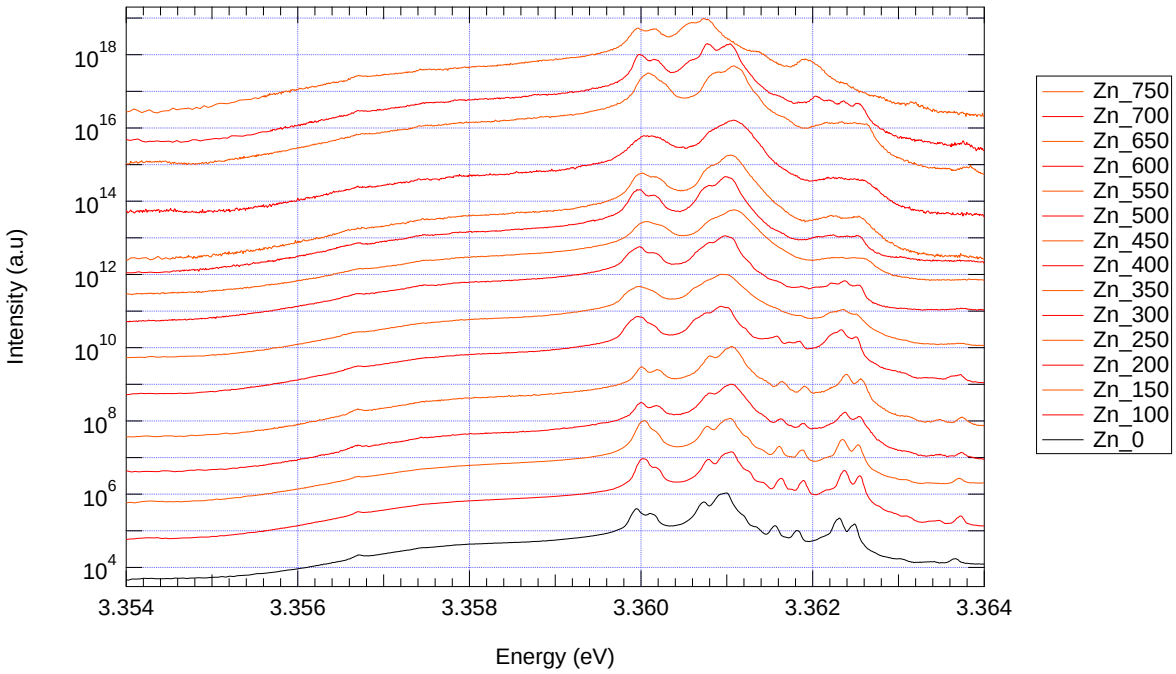

Figure 4.2: Annealing temperature dependent of the expanded donor bound exciton emission of the Zn face of hydrothermal ZnO at 3.9 K. Zn_100 is the Zn face annealed for 90 minutes at 100°C in an O_2 atmosphere.

The spectra in figure 4.1 and figure 4.2 show the near band edge PL of the Zn face of ZnO as the temperature of annealing is increased. The spectra have been vertically displaced to improve visibility. Zn_0 is the reference spectra of the Zn face, increasing height vertically increases the temperature of annealing. The alternating colours represent the two different samples used.

At an annealing temperature of 350°C the hydrothermal hydrogen peak at 3.3624 eV is starting to out gas. At an annealing temperature of 450°C the peak has been completely removed from the spectrum. The assumed Al-H complex centre is not removed at the same temperature. At an annealing temperature of 750°C the Al-H complex centre is out gassed from the sample. This is at a higher annealing temperature than previously seen in figure 3.1. Due to emission having the same energy it is assumed that the Al-H complex centre is the same in both wafers. The difference in annealing temperature implies that the activation energy of the dissociation of the complex is different between wafers. To further investigate the source of this discrepancy the effect of the time of annealing and the accumulation effect of annealing would have to be taken into account.

At an annealing temperature of 450°C the Y-line starts to arise. The intensity of the Y-line increases with annealing temperature from 450°C to 700°C. At an annealing temperature of 550°C the shoulder that is present with the Y_0 line in melt-grown ZnO is identifiable above the background noise. The behaviour of this line is in agreement with the previously annealed wafer shown in figure 3.1.

The B excitons start to be uncovered by the removal of the broad feature between $3.3640 - 3.3740$ eV at an annealing temperature of 500°C. At an annealing temperature of 650°C the structure of the B excitons are most prominent. The removal of the broad feature uncovers the unknown peak at 3.3680 eV with the B excitons. The collection of peaks related to the ionised donors in the region of $3.3715 - 3.3752$

eV broaden at an annealing temperature of 450°C. The cause is possibly due to the combination of the loss of the broad feature and lack of resolution and sample location dependence of this region. The effect of annealing at 600°C in the region $3.3636 - 3.3750$ eV is dramatically different from the spectra shown in figure 3.1.

At an annealing temperature of 750°C the intensity of the neutral donor bound peaks and spectrum overall has sharply decreased in comparison to the reference sample that is attributed to a reduction in crystalline quality. The increase of the intensity of the Y-line from an annealing temperature of 450°C to 700°C is in agreement with this explanation. The intensity loss of the Y-line at annealing temperature of 750°C does not contradict this explanation. This can be asserted as the Y-line is thought to be caused by an exciton bound to an extended structural defect. As the crystalline quality decreases further there could be barriers to excitons propagating to such structural defects thus reducing the Y-line intensity. This could be confirmed with X-ray diffraction with comparison with a reference sample.

There are two peaks at 3.3470 eV and 3.3520 eV that emerge strongly with the removal of the Al-H complex centre at an annealing temperature of 750°C. These peaks could be acceptor bound excitons that are no longer passivated by hydrogen as both hydrogen related peaks have been removed.

At an annealing temperature of 700°C the ratio of the intensities of the free excitons swap and then at an annealing temperature of 750°C the structure and intensity of the free excitons deteriorate completely. This will be linked to the structural quality of the crystal as it deteriorates there will be less ability for the free excitons to form within the lattice.

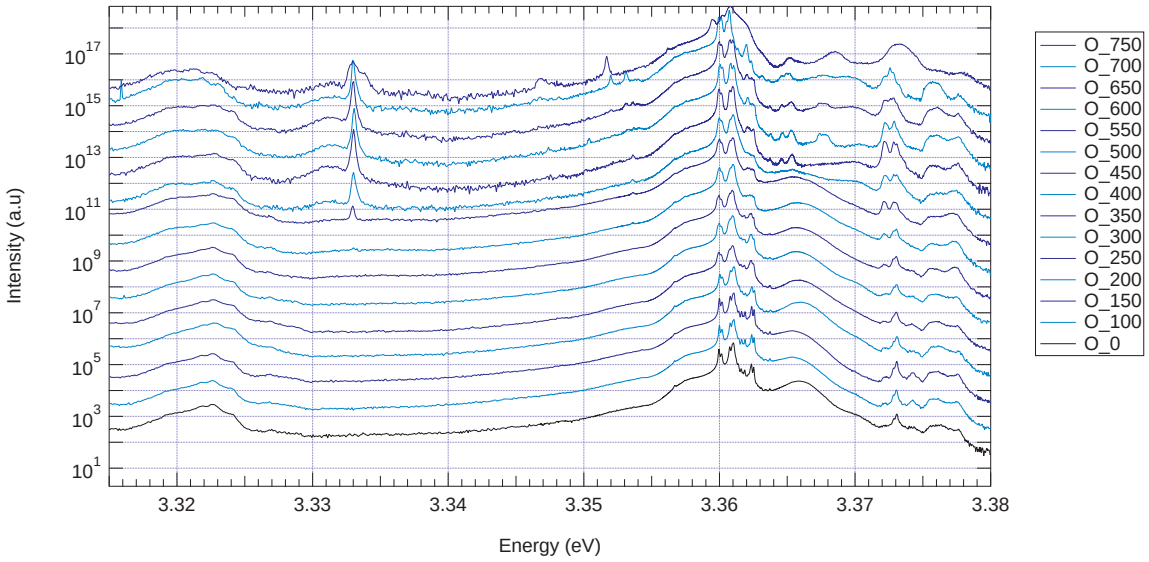

Figure 4.3: Annealing temperature dependent of the near band edge emission of O face of hydrothermal ZnO at 3.9 K. O_100 is the O face annealed for 90 minutes at 100°C in an O_2 atmosphere.

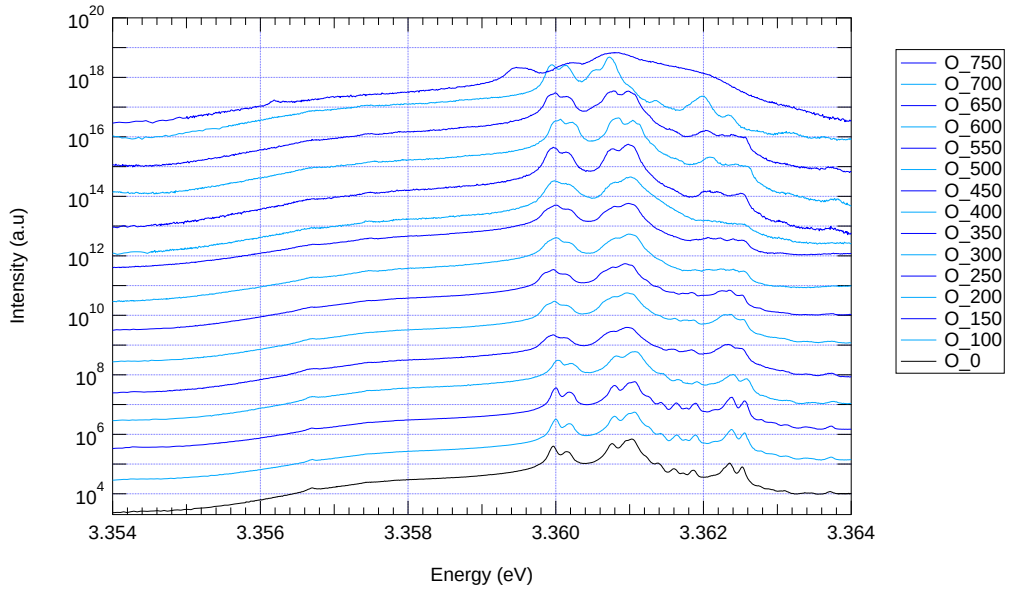

Figure 4.4: Annealing temperature dependent of the expanded donor bound exciton emission of O face of hydrothermal ZnO at 3.9 K. O_100 is the O face annealed for 90 minutes at 100°C in an O_2 atmosphere.

The spectra in figure 4.3 and figure 4.4 show the near band edge of the O face of ZnO as the temperature of annealing is increased. The specta have been vertically displaced to improve visibility. O_0 is the reference spectra of the O face, increasing height vertically increases the temperature of annealing. The alternating colours represent the two different samples used.

On the O face of ZnO the hydrothermal hydrogen peak at 3.3624 eV is out gassed at a lower temperature than the Zn face. With the hydrothermal hydrogen peak starting to out gas at an annealing temperature of 300°C and being completely removed by annealing at 400°C. At an annealing temperature of 700°C the Al-H peak is out gassed on the O face similarly. The change in activation energy is due to a property that is different between the two faces i.e. the surface stabilisation.

With the removal of the two hydrogen peaks possible acceptor bound excitons at 3.3531 eV and 3.3520 eV. At an annealing temperature of 700° these centres are out gassed and peaks at 3.3517 eV and 3.3468 eV appear. All four of these features are located in a region where acceptor bound excitons are theoretically found.

The broad feature in the region $3.364 - 3.374$ eV starts to be removed at an annealing temperature of 500°C. The feature is reduced sufficiently to resolve the B excitons at an annealing temperature of 550°C which is in disagreement with the observation of this feature in figure 3.2 where a different wafer was investigated.

The broad feature in the region $3.3640 - 3.3740$ eV is of unknown origin. This feature is thought to be closely related to the surface of the crystal, as the polarity difference between the $+c$ faces of ZnO is expressed most prominently in this broad feature.

One of the possible causes of the broad surface dependent feature is surface roughness. The free excitons propagate throughout the crystal and when they hit a surface they would reflect or recombine. With a rough surface the energy loss to recombine would be diverse causing a broad feature. The energy loss would also be varied depending on the polarity of the surface as the surface potential is different. This explanation is supported by the activation energy of the removal of the broad

feature being different between wafers.

Evidence against this explanation is shown in spectra taken by Robert Heinhold [2] where a $+c$ Zn face sample is annealed in an O_2 atmosphere then reannealed in forming gas and finally annealed in an O_2 atmosphere. The broad surface dependent feature is removed, recovered with the surface being damaged by the forming gas and then removed without full recovery from the surface damage. The presence of the broad surface related feature on high quality nanowires verifies that it is unrelated to surface roughness [27].

Another possibility for the source of the broad surface dependent feature is the carrier concentration at the surface. This would explain the wafer discrepancy and polarity dependence of the feature. Surface carrier concentration for the O face of ZnO has been shown to be different to that of the Zn face, as the O face has a higher concentration of near surface defects [28]. Annealing of ZnO changes the carrier concentration which would explain the effects different annealing temperatures and atmospheres have on the broad surface related feature. This is supported in spectra taken by Robert Heinhold [2] showing thin layers of metals deposited on ZnO surfaces and how they reduce the broad feature. Such thin metal layers form contacts on the ZnO surface and change the potential through the balancing of the Fermi levels.

In comparison to the unknown Zn face peak at 3.3680 eV, a corresponding peak on the O face does not arise until an annealing temperature of 600°C. The centre of the peak on the O face is located at 3.3676 eV which is slightly red shifted from the Zn face and appears to be made up of a multitude of components. It then reduces with rising annealing temperature until 700°C. At 750°C a peak arises at 3.3685 eV.

In figure 4.1 and figure 4.3 the increase in noise starting at 500°C is due to the loss of intensity overall in the spectra. The cause of the loss of intensity is a convolution of actual loss of intensity of emission due to reduction in crystal quality and non-optimal experimental conditions. The optimisation of the optics in this series of spectra did not take into account the mounting of the samples. The samples are mounted using silver paste as an adhesive. The depth of silver paste used was non-uniform causing the samples not to lie in the same plane. As the plane the samples lay in changed the collection optics for differing samples requires re-optimisation.

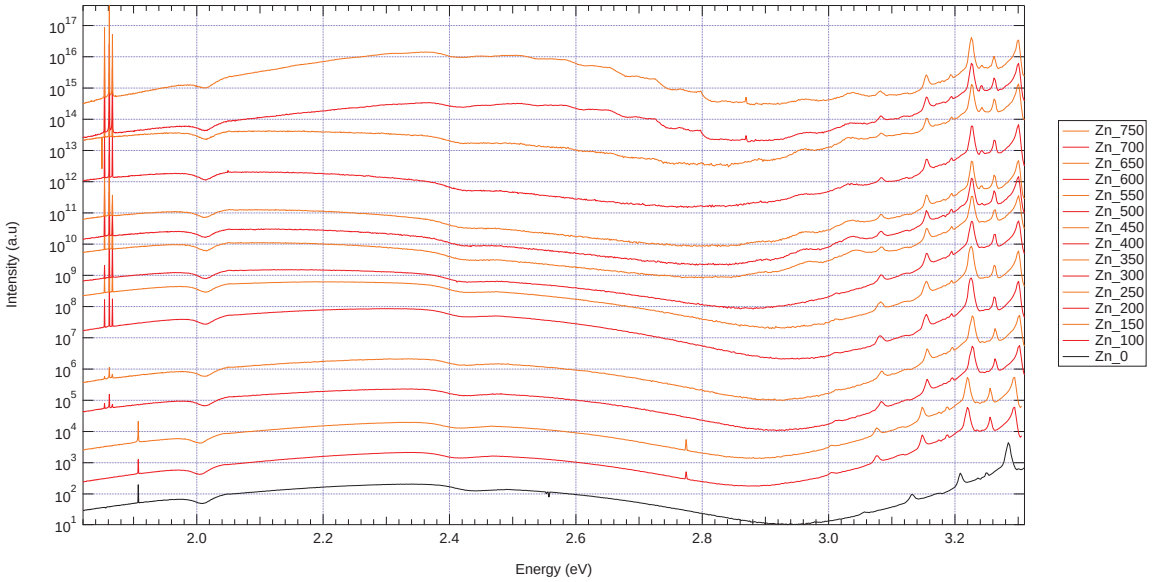

Figure 4.5: Annealing temperature dependent of the defect band emission of Zn face of hydrothermal ZnO at 3.9 K. Zn_100 is the Zn face annealed for 90 minutes at 100°C in an O_2 atmosphere.

The spectra in figure 4.5 and figure 4.6 show the defect band of the Zn face of ZnO as the temperature of annealing is increased. The spectra have been vertically displaced to improve visibility. Zn_0 is the reference spectra of the Zn face and increasing height vertically increases the temperature of annealing. The alternating colours represent the two different samples used.

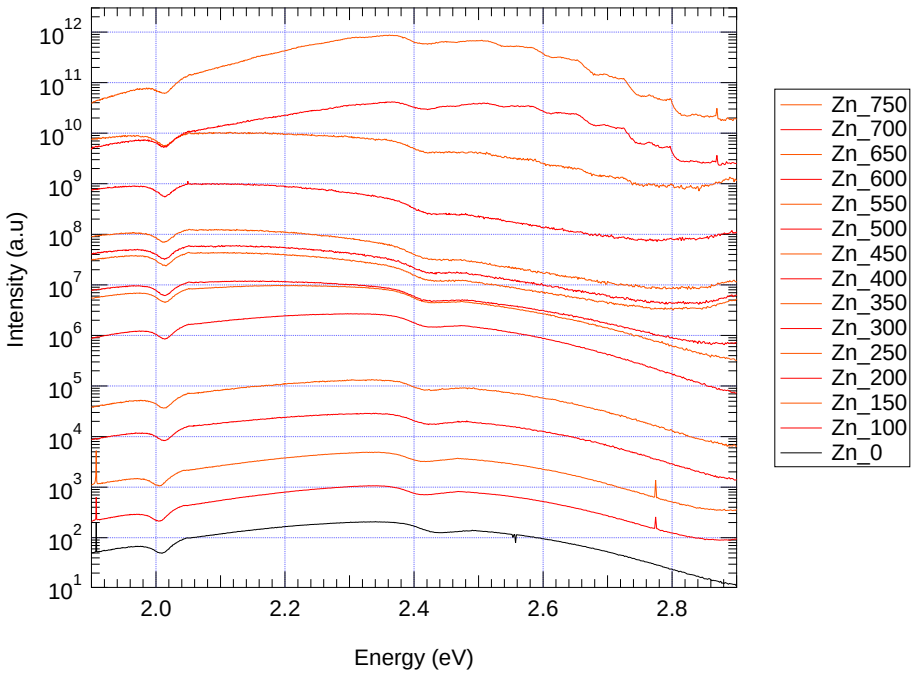

Figure 4.6: Annealing temperature dependent of the visible defect band emission of Zn face of hydrothermal ZnO at 3.9 K. Zn_100 is the Zn face annealed for 90 minutes at 100°C in an O_2 atmosphere.

The change in excitation source can be clearly seen by the change in the doubled laser line emission at 1.9074 eV and plasma line at 2.7862 eV for the HeCd laser for annealing temperatures of 100°C, 150°C and the reference sample of Zn_0; and the argon laser with an emission at 1.8583 eV for all other lines. The dip features at 2.013 eV and 2.408 eV are due to artifacts arising from the diffraction grating in the spectrometer.

The defect band emission of ZnO is in the visible luminescent region. This visible emission can be described as two broad luminescent centres one red and one green. Up to an annealing temperature of 300°C the emission is dominated by the broad green feature. The broad green feature has been related to copper ions (Cu^{+}) [29]. Above the annealing temperature of 300°C the emission of the broad green feature is reduced and the broad red feature is increased. At 650°C the broad red feature is diminished and the green broad feature exhibits structural steps which have been related to copper ion (Cu^{2+}) [29].

At an annealing temperature of 450°C in the region $2.8500 - 3.0500$ eV peaks form that could be related to donor-acceptor pair recombination. The appearence of these peaks at 450°C is expected with the removal of the hydrothermal hydrogen centre, as hydrogen is thought to passivate acceptors that appear in figure 4.1. The formation of donor-acceptor pair recombination emission before acceptor bound excitons are observed in the near band edge region suggests passivation is still occurring. This is substantiated by the retention of the Al-H complex up to 450°C. As previously discussed there are two peaks at 3.3470 eV and 3.3520 eV that could be acceptors appear at an annealing temperature of 750°C. However the emergence of these acceptor peaks is not correlated with an increase in the donor-acceptor pair recombination as would be expected. The deficiency could be caused by the decrease in crystalline quality affecting the donor-acceptor pair transitions to a greater extent.

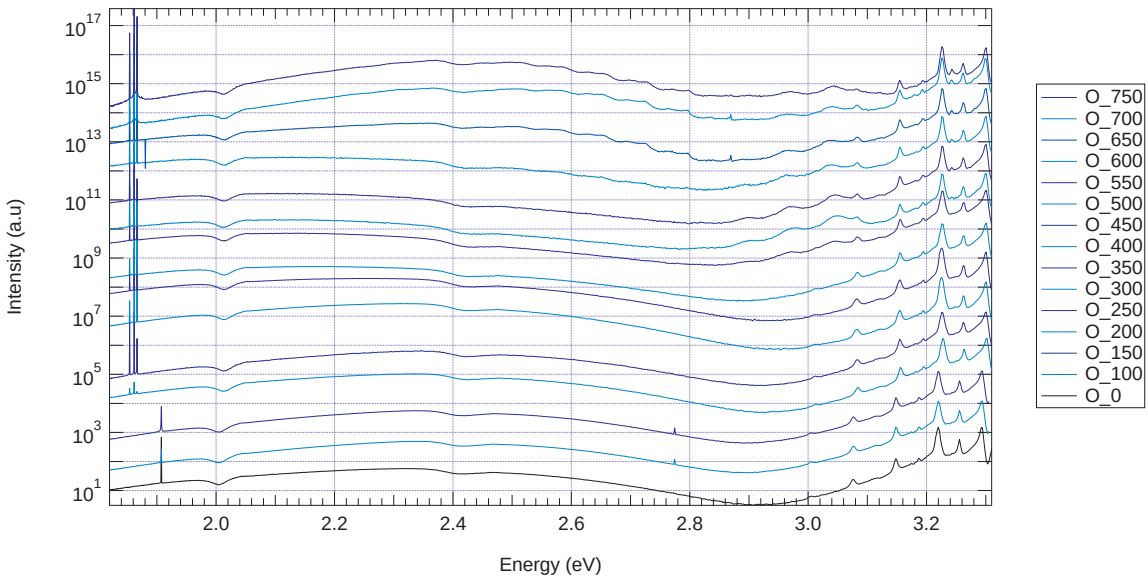

Figure 4.7: Annealing temperature dependent of the defect band emission of O face of hydrothermal ZnO at 3.9 K. O_100 is the O face annealed for 90 minutes at 100°C in an O_2 atmosphere.

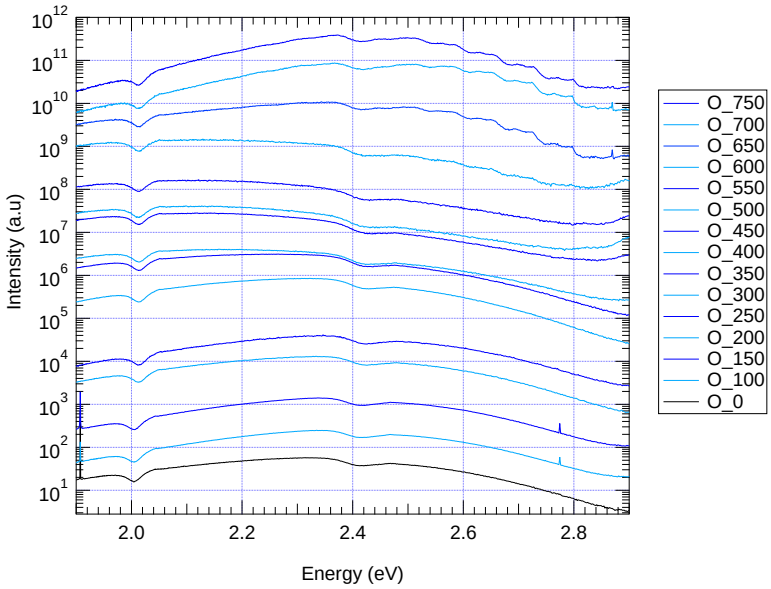

Figure 4.8: Annealing temperature dependent of the visible defect band emission of O face of hydrothermal ZnO at 3.9 K. O_100 is the O face annealed for 90 minutes at 100°C in an O_2 atmosphere.

The spectra in figure 4.7 and figure 4.8 show the defect band of the O face of ZnO as the temperature of annealing is increased. The specta have been vertically displaced to improve visibility. O_0 is the reference spectra of the O face, increasing height vertically increases the temperature of annealing. The alternating colours represent the two different samples used.

At an annealing temperature of 400°C peaks that could be related to donor-acceptor pair recombinations occur in conjunction with the removal of the hydrothermal hydrogen centre shown in figure 4.3. The possible acceptor bound excitons in the O face cannot be correlated with these donor-acceptor pair recombinations as with the Zn face.

The behaviour of the broad visible feature on the O face of ZnO is different to that in the Zn face. At an annealing temperature of 300°C the broad red feature is increased while the broad green feature remains constant. At 600°C the structure of the broad green feature related to Cu^{2+} starts to appear with the broad red feature starting to reduce at 650°C. The differing behaviour of the Zn and O face in the

defect band support the argument of different carrier concentration from altered collections of impurities within the crystal surfaces.

Chapter 5

Time dependent annealing

The time of annealing is not generally looked at in annealing studies. In this thesis the effect of the time of annealing is investigated by keeping the temperature and atmosphere of annealing constant and looking at the PL of samples as a function of accumulated annealing time. The Zn and O faces of $+c$ hydrothermal ZnO were investigated by PL analysis for every 15 minutes of annealing at 600°C in an O_2 atmosphere. The HeCd laser was the excitation source for the annealing time dependent PL analysis.

The spectra in figure 5.1 and figure 5.2 show the near band edge PL of the Zn face of ZnO as the time accumulated during annealing is increased. Zn_R is the reference spectra of the Zn face, increasing height vertically increases the annealing time. The alternating colours are for visibility.

The peak with an emission energy of 3.3535 eV is in the region where acceptor bound excitons are thought to be located. This peak appears at 15 minutes annealing time and after 30 minutes it is further enhanced. After 45 minutes the intensity of the emission is slightly reduced and remains constant for extended annealing time. An interpretation of what is occurring is at 30 minutes annealing time all the hydrogen that is passivating the acceptors is removed along with the near surface defects that could screen the acceptors. For accumulated annealing times greater then 30

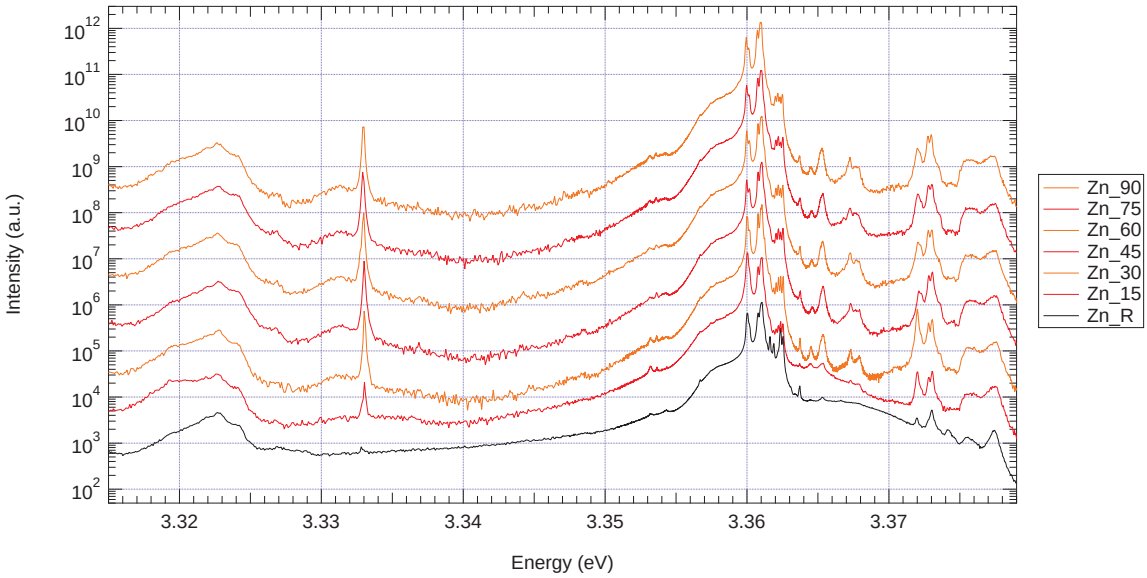

Figure 5.1: Annealing time dependence PL of the near band edge emission of the Zn face of hydrothermal ZnO at 3.9 K. Zn_15 is the Zn face annealed for 15 minutes at 600°C in an O_2 atmosphere.

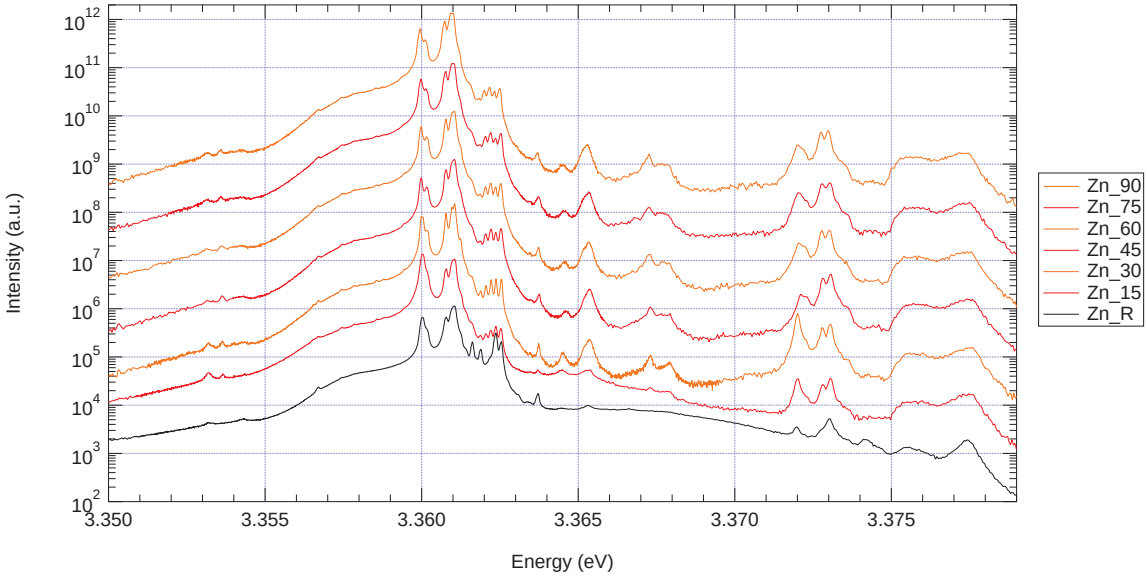

Figure 5.2: Annealing time dependence PL of the tight near band edge emission of the Zn face of hydrothermal ZnO at 3.9 K. Zn_15 is the Zn face annealed for 15 minutes at 600°C in an O_2 atmosphere.

minutes the acceptors are starting to be out gassed giving a consistent but lower concentration then is previously present as acceptors move from the bulk into the region sampled by PL and then are out gassed. As previously discussed in chapter 3 high temperature annealing has been shown to migrate Li to the surface. It should be noted that Li is a light element and the acceptors present may be heavier. The tem-

perature used to migrate Li to the surface is also significantly greater then used here.

The broad unknown feature at 3.3672 eV is shown in higher resolution than in the temperature dependent or atmosphere dependent annealing. This higher resolution shows that it is a collection of centres causing emission in this region. As a function of annealing time the ratio of intensity of emission from these centres change as a function of time. This variation could be related to defects being out gassed.

At accumulated annealing times of 15 and 30 minutes a feature at 3.3720 eV appears. This feature has been previous related in section 2.2 figure 2.3 to the location of the laser spot on the sample.

After 30 minutes annealing time the remainder of the spectrum becomes consistent. The Y-line at 3.3330 eV having a constant intensity with accumulated annealing times greater than 30 minutes is of interest as this implies that an annealing temperature of 600°C creates a limited number of extended structural defects in the sample. The temperature dependent annealing in chapter 4 show a constant increase in the Y-line with an annealing temperature indicating no limit to the extended structural defects with increasing thermal treatment. This could be speculated to indicate that there are a limited number of defects, with different thermal activations in the crystal, that the extended structural defects propagate from. This agrees with the discussed possible anticorrelation between point defects and extended structural defects [23].

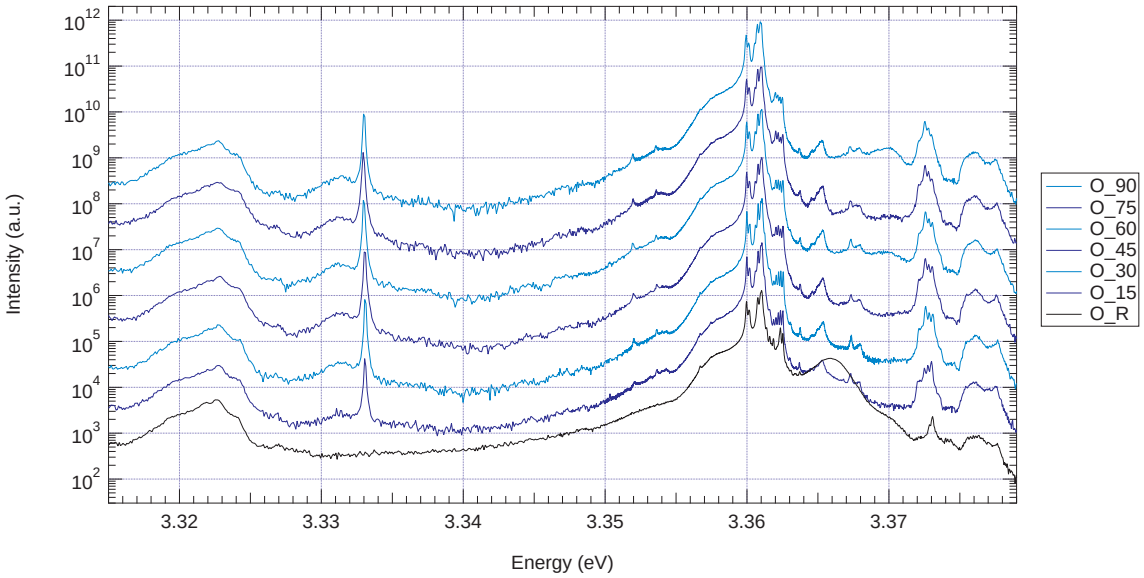

Figure 5.3: Annealing time dependence PL of the near band edge emission of the O face of hydrothermal ZnO at 3.9 K. O_15 is the O face annealed for 15 minutes at 600°C in an O_2 atmosphere.

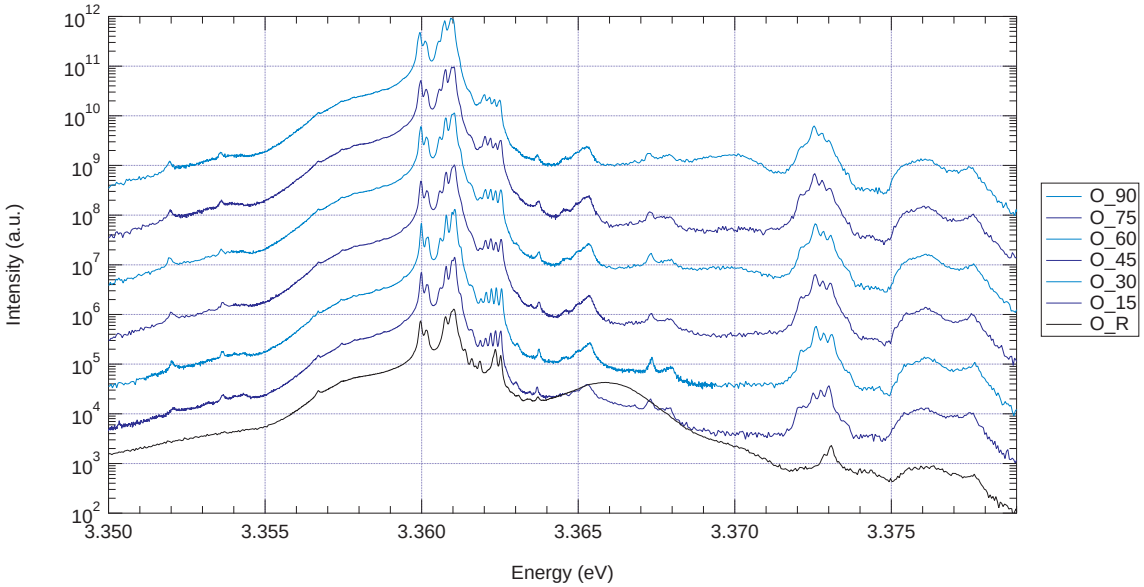

Figure 5.4: Annealing time dependence PL of the tight near band edge emission of the O face of hydrothermal ZnO at 3.9 K. O_15 is the O face annealed for 15 minutes at 600°C in an O_2 atmosphere.

The spectra shown in figure 5.3 and figure 5.4 shows the near band edge of the O face of ZnO as the time accumulated during annealing is increased. O_R is the reference spectra of the O face, increasing height vertically increases annealing time. The alternating colours are for visibility.

The ratio of the intensity of the peaks in the ionised donor region $3.3716 - 3.3739$ eV change as a function of annealing time on the O face. The collection of peaks is similar to the ionised donor region seen on the O face during temperature dependent annealing at annealing temperatures of 650°C and 700°C. The features in this region that have not previously related to ionised donors have different thermal activations depending on the sample within a wafer. The emission is this region has already shown a dependence on the sampling location on the wafer in figure 2.3. The previous correlation between the ionised donors and the neutral donor bound excitons is still valid. In contrast to the Zn face, after 15 minutes the remainder of the O face spectra become consistent.

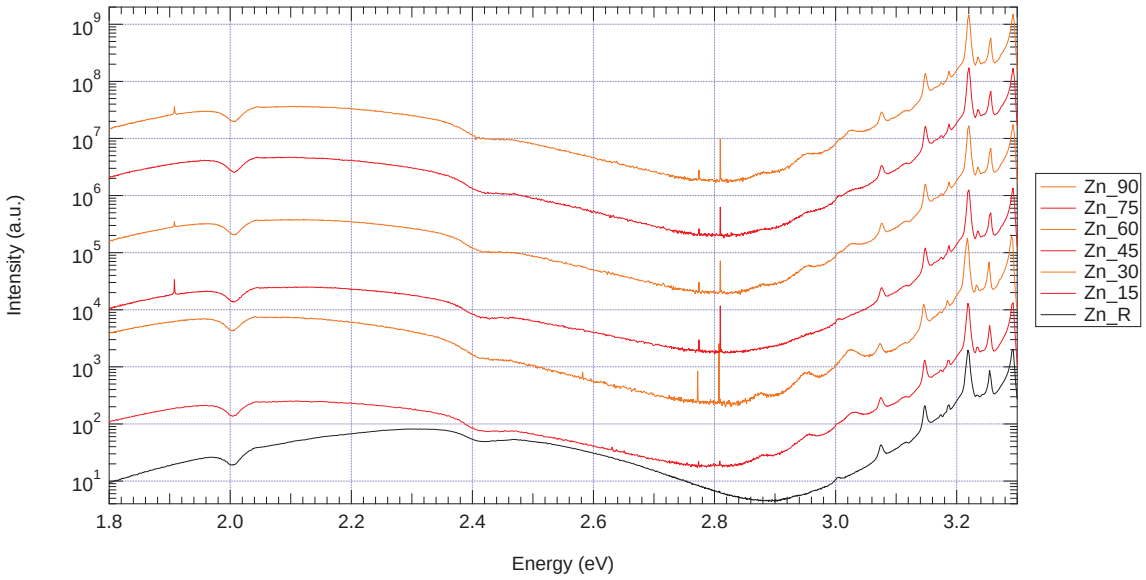

Figure 5.5: Annealing time dependence PL of the defect band emission of the Zn face of hydrothermal ZnO at 3.9 K. Zn_15 is the Zn face annealed for 15 minutes at 600°C in an O_2 atmosphere.

The spectra in figure 5.5 show the defect band edge of the Zn face of ZnO as the time accumulated during annealing is increased. Zn_R is the reference spectra of the Zn face, increasing the height vertically increases annealing time. The alternating colours are for visibility.

The peaks thought to be related to donor-acceptor pair recombinations can be observed to show behaviour that can be correlated with the acceptor peaks in the near band edge. The exception of this is their intensity at accumulative annealing times of 45 and 75 minutes where they are greatly diminished in intensity.

The sharp features at 2.8074 eV and 2.7722 eV are plasma lines of the HeCd lasers. They appear more prominent here than in earlier spectra because of an increase in spectral resolution through that region and the refurbishment of the HeCd laser.

After an accumulative annealing time of 30 minutes the remainder of the spectrum becomes consistent. There is a reduction of the intensity of the broad green feature and a increase in the intensity of the broad red feature from the reference spectra.

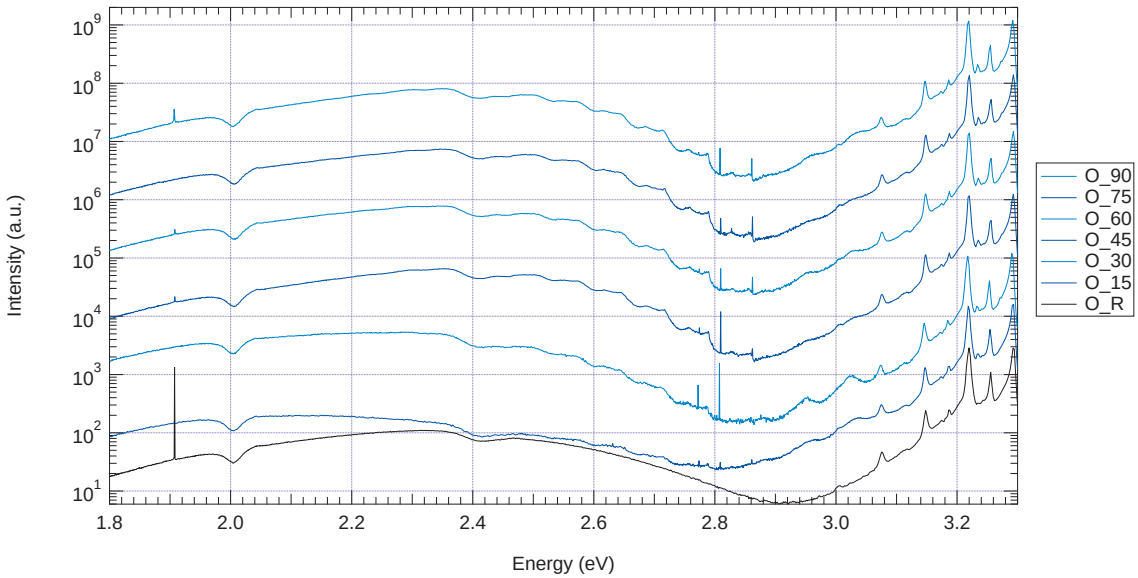

Figure 5.6: Annealing time dependent PL of the defect band emission of the O face of hydrothermal ZnO at 3.9 K. O_15 is the O face annealed for 15 minutes at 600°C in an O_2 atmosphere.

The spectra in figure 5.6 show the defect band of the O face of ZnO as the time accumulated during annealing is increased. O_R is the reference spectra of the O face, increasing height vertically increases the time spent annealing. The alternating colour is to improve visibility.

The intensity of the donor-acceptor pair recombination in the region $2.9000 - 3.0800$ eV display the behaviour observed for the Zn face with increase of intensity for increased accumulated annealing time until 30 minutes and then a reduction to a consistent intensity for greater annealing times. This along with the observations of the Zn face defect band give evidence that the peaks seen in the near band edge of both faces of ZnO in the region around 3.3535 eV are not the acceptors that are related to the donor-acceptor pair recombination seen in this region.

The broad visible feaures display different behaviour for the O face in comparison to the Zn face, as with temperature dependence. After 15 minutes annealing the definition in the copper steps in the region $2.48 - 2.81$ eV starts to occur. At an accumulative annealing time of 45 minutes they have reached a maximum intensity which is maintained for the rest of annealing. The broad red feature remains untouched.

As shown in figures 5.1 and 5.3 the spectra taken during time dependent annealing has resolved the fine structure remaining in the location of the removed hydrothermal hydrogen feature at 3.3624 eV.

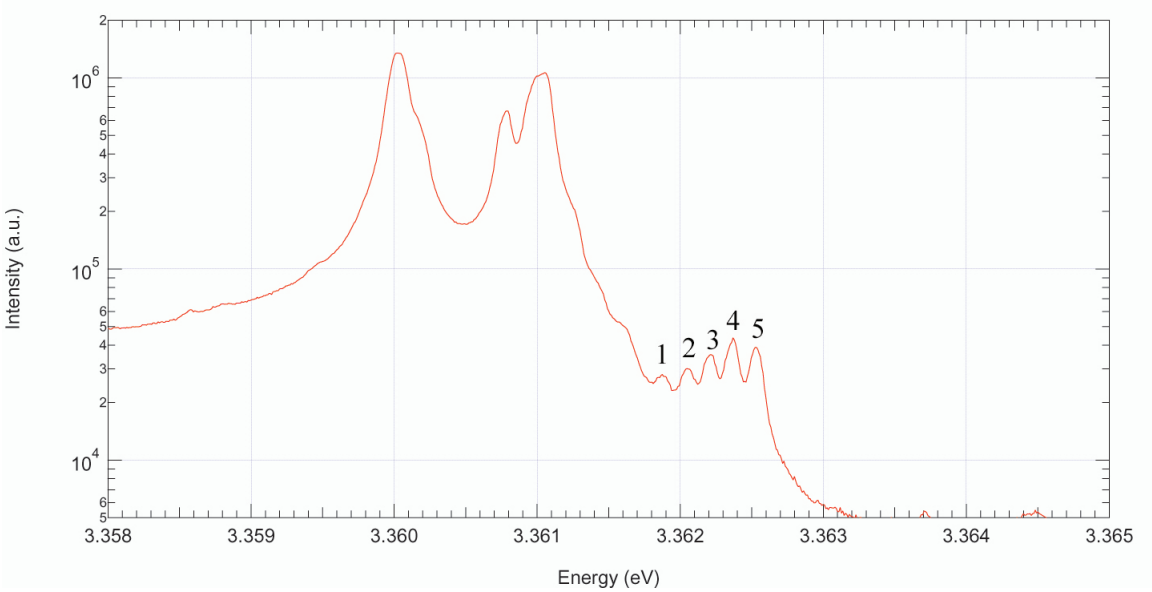

Figure 5.7: Donor bound excitons of the Zn face of hydrothermal ZnO that has been annealed at 600°C for 15 minutes in an O_2 atmosphere. The fine structure has been labelled.

Figure 5.7 shows Zn face $+c$ bulk ZnO that has been annealing in O_2 at 600°C for 15 minutes. The fine structure present is labelled $1-5$ from left to right for convenience. Temperature dependent PL was carried out to investigate the nature of this fine structure uncovered under the hydrothermal hydrogen peak.

The spectra in figure 5.8 show the temperature dependence of the 5 peaks uncovered under the removed hydrothermal hydrogen peak. Due to the additive nature of PL and the proximity of the peaks the integrated intensity could not be extracted. Therefore the intensity used for the Arrhenius plots discussed below is the just the intensity maximum of the peaks and this data is presented in figure 5.9.

As seen in figure 5.9 (a) there was sufficient clarity to analyse the temperature dependence of only three of the peaks as the fine structures quickly become convoluted by thermal broadening making identification difficult. The three peaks with sufficient data display an increase in intensity with temperature.

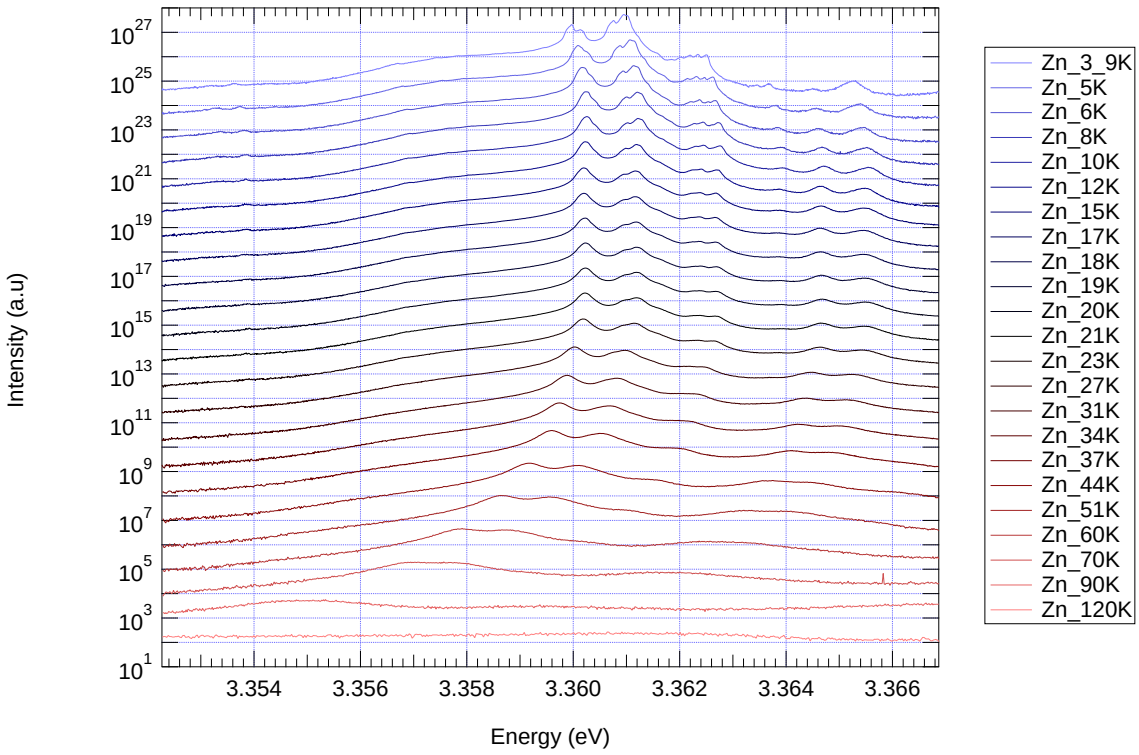

Figure 5.8: Temperature dependent PL of the near band edge emission of the Zn face of ZnO annealed at 600° for 15 minutes in an O_2 atmosphere.

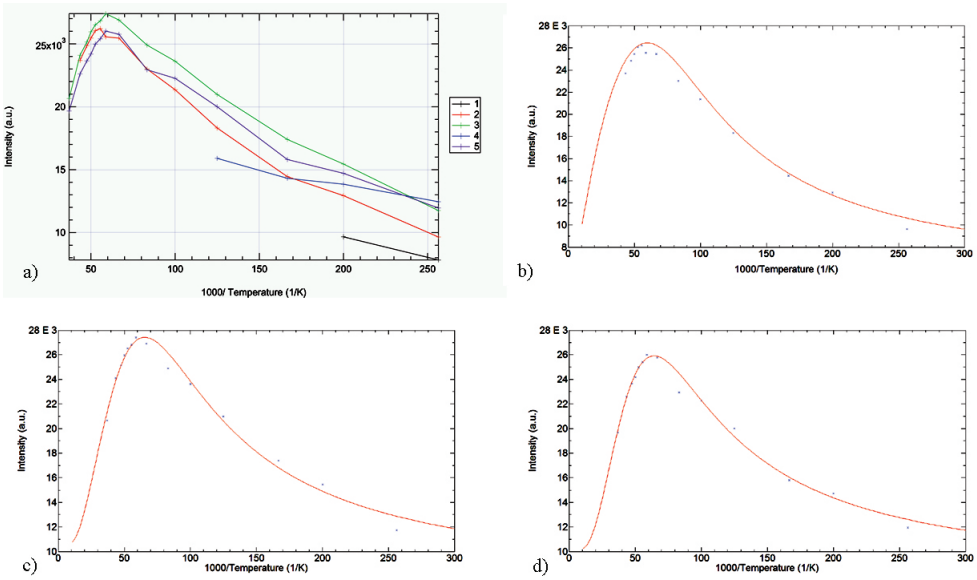

Figure 5.9: a) Arrhenius plots for all 5 peaks, b) Fitted Arrhenius plot for peak 2, c) Fitted Arrhenius plot for peak 3, d) Fitted Arrhenius plot for peak 5.

Figure 5.9 (b),(c) and (d) show the fitting of equation 1.1 for the peaks 2, 3 and 5 respectively. For fitting using equation 1.1 $w = 1$ was used as the negative thermal quenching (increase in intensity with temperature) as it is assumed there is only

one mechanism of activation. Similarly, $m = 1$ was used as the thermal quenching would be dominated by the single quenching of the ground state.

For the equation a value of $I(0)$ is required as the model assumes that towards 0 K the emission intensity of an excited state plateaus. The data shows that even at the lowest temperature used there is still significant change in intensity as reflected by the presence of a gradient to the data at high values of inverse temperature. Rather than allowing $I(0)$ to be a free parameter in the Arrhenius fit, a range of fixed $I(0)$ values were set. An average value was then determined from sufficiently small χ^2 values. The weighting parameters C and D were varied as initial conditions in an attempt to improve accuracy. The resulting parameters found are the average of sufficiently accurate fits. The fitting was done in MATLAB using code shown in Appendix I.

Fine structure line label	$I(0)$ (a.u.)	$D1$	$E1$ (meV)	$C1$	$E2$ (meV)
2	$7 \pm 2 \times 10^3$	4 ± 1	2.4 ± 0.2	7.20 ± 0.07	23.20 ± 0.04
3	$11 \pm 1 \times 10^3$	5.3 ± 0.4	5.2 ± 0.4	8.5 ± 0.4	21.22 ± 0.06
5	$10 \pm 2 \times 10^3$	6.6 ± 0.6	6.0 ± 0.9	9 ± 1	19.8 ± 0.2

Table 5.1: Parameters from equation 1.1 for thermal behaviour of the fine structure.

Table 5.1 shows the parameters found with the uncertainty for each of the three PL lines. The activation energies for the thermal quenching parameter $E2$ are on the order of 20 meV. Which here is considered to be the activation energy of the thermal quenching of the ground state. The fitting of a negative thermal quenching model to the three features confirmed the peaks to be excited states of bound excitons.

The activation energy of the negative thermal quenching mechanism could be correlated with the splitting between the excited state and its ground state. Using this argument the peaks labelled 3 and 5 can be associated with the neutral donor bound exciton at 3.3567 eV, labelled as I_9 in the literature, as it resides at an energy

of $E1$ to the fine splitting peaks 3 and 5. The peak labelled 2 with $E1 = 2.4$ meV does not correlate with any other low energy feature in this way. Either the parent ground state transition for peak 2 is hidden or a more sophisticated model is required.

Rotational and vibrational excited states of neutral donor bound excitons have been previously identified in ZnO by magneto-PL and PLE measurements [24]. These excited states can be calculated by equation 1.3 and might be the experimentally observed fine structure introduced above.

Bound exciton	Energy (eV)	Localisation Energy (meV)	E(0, 0) (meV)	ν	J	Energy above ground state (meV)	Excited state energy (eV)
I	3.3567	19.1	3.03	0	1	2.04	3.35874
				1	0	2.14	3.35884
				1	1	2.58	3.35928
				0	2	2.57	3.35927
				2	0	2.61	3.35931
				1	2	2.77	3.35947
				2	1	2.78	3.35948
				2	2	2.87	3.35957
II	3.3600	15.8	2.18	0	1	1.49	3.36149
				1	0	1.55	3.36155
				1	1	1.87	3.36187
				0	2	1.86	3.36186
				2	0	1.89	3.36189
				1	2	2.00	3.36200
				2	1	2.00	3.36200
				2	2	2.07	3.36207
III	3.3601	15.7	2.16	0	1	1.47	3.36157
				1	0	1.54	3.36164
				1	1	1.85	3.36195
				0	2	1.84	3.36194
				2	0	1.87	3.36197
				1	2	1.98	3.36208
				2	1	1.98	3.36208
				2	2	2.04	3.36214
IV	3.3608	15.0	1.99	0	1	1.37	3.36217
				1	0	1.42	3.36222
				1	1	1.71	3.36251
				0	2	1.70	3.36250
				2	0	1.72	3.36252
				1	2	1.83	3.36263
				2	1	1.83	3.36263
				2	2	1.89	3.36269
V	3.3610	14.8	1.94	0	1	1.33	3.36233
				1	0	1.39	3.36239
				1	1	1.67	3.36267
				0	2	1.66	3.36266
				2	0	1.68	3.36268
				1	2	1.79	3.36279
				2	1	1.79	3.36279
				2	2	1.84	3.36284

Table 5.2: Vibrational and rotational excited states of neutral donor bound excitons in the Zn face of hydrothermal ZnO annealed at a temperature of 600°C in an O_2 atmosphere for 15 minutes at 3.9 k calculated using equation 1.3.

Table 5.2 shows the vibrational and rotational excited states of the experimentally found neutral donor bound excitons calculated using:

$$E(\nu, J) = \frac{-(2ma^2/\hbar^2)D^2}{\left[\left(\nu+\frac{1}{2}\right)+\sqrt{\left(J+\frac{1}{2}\right)^2+\left(\frac{2ma^2}{\hbar^2}\right)D}\right]^2}$$

The factors m and a are being taken from Meyer et al [24]. With $m = 0.7m_0$ and $a = 0.8$ nm, where m_0 is the mass of an electron. The weighting of these factors in the calculation of the meV shifts is quite pronounced so the uncertainty of the calculated values could be substantial. The quantum numbers ν and J covered only a small range $0-2$ as for higher values the difference between excited states becomes smaller than the resolution of the spectra. The MATLAB code used to calculate the excited states is shown in Appendix II.

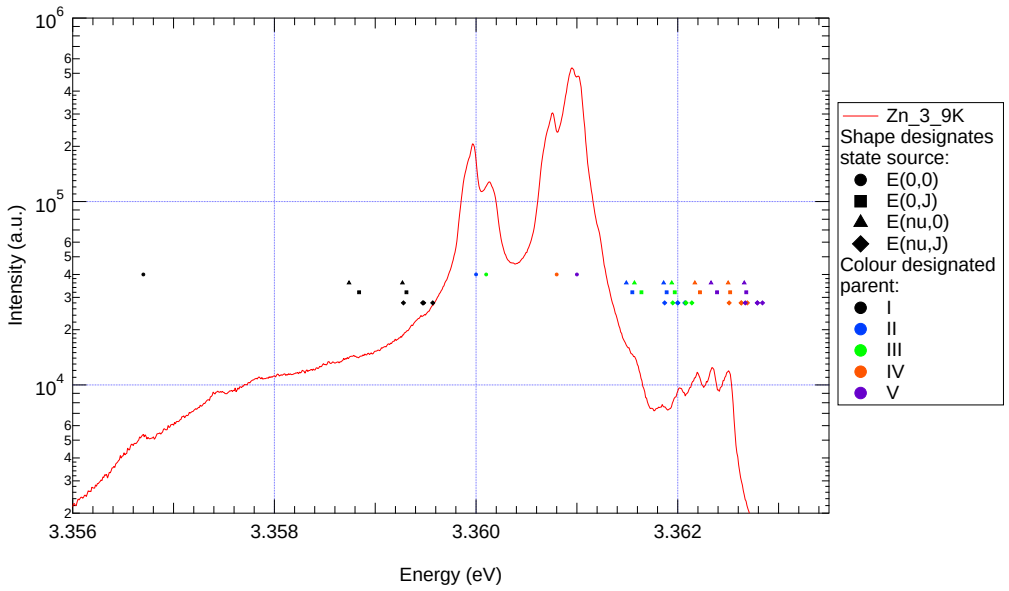

Figure 5.10: Vibrational and rotational excited states of the neutral donor bound excitons. The spectrum is from the Zn face of hydrothermal ZnO annealed at a temperature of 600°C in an O_2 atmosphere for 15 minutes at 3.9 k.

The calculated energy shifts to these excited vibrational and rotational states from parent lines that are in table 5.2 are superimposed on the spectra shown in figure 5.10. The colour of the symbols designate the ground state they originate from while the shape designates whether it is vibrational, rotational or both.

The first thing apparent from figure 5.10 is that a multitude of closely spaced PL lines could be observed when this excited state model is considered. There is evidence that only singularly rotational or singularly vibrational states might be the cause of the features. The combined vibrational and rotational excited states do not appear to be present in the spectra. This demonstrates that if this fine structure PL are vibrational and rotational excited states, then selection of the quantum numbers is occurring.

It is acknowledged that associating this fine structure with excited states of donor bound excitons is uncertain without additional evidence. Another test would be comparing their intensity ratios with other samples that exhibit different overall donor bound exciton structure as there should be internal consistency.

5.1 Wafer dependency of high resolution ZnO photoluminescence

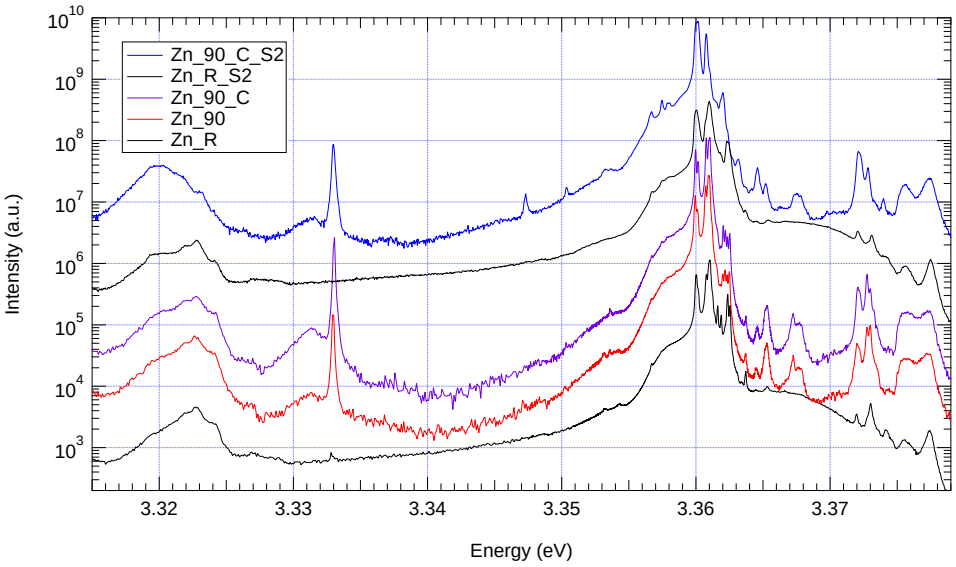

Figure 5.11: Wafer dependence of annealing effect on PL.

Figure 5.11 demonstrates the disparity between the two different wafers used in the experiments. All spectra was taken at 3.9 K. Zn_R is the reference Zn face sample from the hydrothermal ZnO wafer labelled S1 used in time dependent and temperature dependent annealing experiments. Zn_90 is a Zn face sample from S1 that was annealed in an O_2 atmosphere at 600°C at 15 minute time intervals up to an accumulated annealing time of 90 minutes. Zn_90_C is a Zn face sample from S1 that was annealed in an O_2 atmosphere at 600°C for 90 minutes. Zn_R_S2 is the reference Zn face sample from the hydrothermal ZnO wafer labelled S2 used in atmospheric dependent annealing experiment. Zn_90_C_S2 is a Zn face sample from S2 that was annealed in an O_2 atmosphere at 600°C for 90 minutes. The variation in resolution between the spectra of the two different wafers is due to an increase in the quality of experimental technique.

Sample S2 demonstrates a larger more intense population of peaks in the acceptor bound exciton region near 3.3570 eV after annealing than the other sample.

This implies a higher concentration of defects in S2 which would effect the carrier concentration. This agrees with the observations of the broad surface feature in the near band edge region on the O face of ZnO in figures 5.3 and 3.2. The shape of the unknown feature at 3.3672 eV has different intensity ratios between the two different samples. This shows that the cause of this unknown feature is wafer dependent and is probably a defect in the ZnO crystal.

The B excitons at 3.364 eV and the ionised donor bound excitons at 3.373 eV correlate their intensities very well with the neutral donor bound excitons in the two wafers. The possible vibrational and rotational excited states of the neutral donor bound exciton peaks discussed above are not resolved in sample S2 so no additional information can be found.

Chapter 6

Summary

Bulk hydrothermal ZnO grown by Tokyo Denpa has been analysed with high resolution PL at 3.9 K. Samples cut from two different wafers have been examined after being annealed while altering the time, temperature and atmosphere annealing parameters.

The splitting displayed by the Al neutral donor bound exciton complex at 3.3608 eV has been related to an Al-H complex by its behaviour under the different atmospheres during annealing and hydrogen implantation. The Al-H complex is observed to have different thermal activation for out gassing from different wafers. This is presumably caused by different carrier concentrations within the samples.

The broad feature in the near band edge in the region $3.3640 - 3.3740$ eV has been related to the surface defects of the crystal changing the carrier concentration. Future work to confirm this connection would be a temperature dependent annealing series of the O face of ZnO while being analysed by PL along with depth-resolved cathodoluminescence spectroscopy and temperature dependent resistivity. Such an experiment would allow for the concentration and depth of surface defects to be monitored in conjunction with the broad surface feature in the near band edge as it changes.

The new Al-H splitting was found to confirm the identification of the excitons bound to ionised donors and bound excitons with the hole in the B-valence band. This was done through a consistent relative intensity profile of the associated peaks. The relationship is further confirmed by the wafer dependence, as the different wafers show different intensity ratios for the neutral donor bound excitons which are repeated in the ionised donors and B excitons.

The fine structure under the hydrothermal hydrogen between $3.3618 - 3.3627$ eV has been confirmed as excited states of bound excitons by temperature dependent PL and fitting negative thermal quenching behaviour. A model based on the Kratzer potential was able to produce the small splittings required. This model using vibration and rotational quantum numbers produces excited states of donor bound excitons. The fine structure could possibly be vibrational and rotational excited states of the donor bound excitons if selection of quantum numbers is occurring. PL of similar resolution or greater than that used in the time dependent annealing series could support or disprove the theory. Confirmation would come from observing consistent intensity ratios of the fine structure and their parent donor-bound exciton peaks across a range of wafers.

The unknown feature at 3.3672 eV has been related to defects within the crystal as the intensity ratio differs between wafers, with temperature dependent annealing and time dependent annealing.

The Y-line extended structural defect show evidence it is related to structural defects already present within the crystal as it remains constant after 30 minutes of accumulative annealing time. The temperature dependent annealing show a constant increase in the Y-line. This could be speculated to indicate that there is a limited number of defects with different thermal activations in the crystal that the extended structural defects propagate from.

The broad multi-component visible feature is closely linked to the defects within the crystal before annealing, with the Cu PL feature having a higher prominence on the O face. Oxygen vacancies have been reported to be deep defects within ZnO which could be related to the broad red feature. This could be investigated with positron annihilation spectroscopy which can investigate vacancies in crystalline structures.

The possible donor acceptor pair recombination seen in the range of $2.8600 - 3.1300$ eV could be investigated with power dependent PL. The emission is expected to blue shift as a result of the decrease in the distance between donor and acceptor of a pair with increasing excitation intensity [30]. Magneto-spectroscopy of the samples could be used to help identify the acceptor bound excitons in the near band edge of ZnO as they differ in how the conduction and valence bands interact with the energy levels of the defects.

The annealing work in this thesis could be extended with ion implantation. Annealing of ion implanted samples is carried out to recover damage from the implantation process. The effect of annealing on the optical properties of undoped ZnO will help isolate the optical effect of the implanted ion . The help the work in this thesis will provide is limited as the investigated samples were not damaged similarly to samples with implanted ions. To remove this limit the ZnO samples investigated will have to be damaged. Damaging of undoped ZnO to an equivalent state will prove difficult as ZnO is radiation hard.

Chapter 7

Appendix: Matlab Code

7.1 Appendix I

The code used to fit negative thermal quenching:
The main code that is initiated for fitting

```
\%\% Fitting negative thermal quenching
\% using the function I=IO*((1+D1.*exp(-E1./(kb.*x))./(1+C1.*exp(-E2./(kb.*x))));
\% with m and w = 1, ie only one NTQ responce and one  TQ responce
\% version 5 (1/2/2014)
\%
\%
\%\% Clearing old data
clc
clear all

\%\% Checking user has input relivant data for fitting

answer = input('Have you inserted your data in the m file? Y/N [Y]: ','s');
if answer== 'Y'

elseif answer== 'y'

else
    error('Error Input Data')
end

\%\% Input your Experimental data below
global x y IO1 IO2 IO3 IO4 IO5 IO6 IO7 IO8 IO9 IO10
\% y= intensity
y=[11744,15448,17403,20978,23622,24901,26893,27400,26822,26521,25958,25150,24094,20659];
\% x= 1/temperature
x=[256.410,200.000,166.667,125.000,100.000,83.3333,66.6667...
    ,58.8235,55.5556,52.6316,50.000,47.619,43.4783,37.037];

\%\% Checking data is the same length and creating array for moddeling

a=length(y);
aa=length(x);
```

```
xx=(max(x)+100):-1:(10);
if a == aa
else
    error('Error Array Lengths Different')
end


\%\% Setting 10 values for IO and 2 sets of parameters

\%Setting IO values
IO10=min(y);
IO9=0.9*min(y);
IO8=0.8*min(y);
IO7=0.7*min(y);
IO6=0.6*min(y);
IO5=0.5*min(y);
IO4=0.4*min(y);
IO3=0.3*min(y);
IO2=0.2*min(y);
IO1=0.1*min(y);
\%the weighting parameters D1=10, C1=1
\%the activation energy of NTQ=5 as physically close
\%the activation energy of TQ=20 as physically close
guessparams1=[10,5,1,20];
\%swapping weightings incase local minimum is found
\%the weighting parameters D1=1, C1=10
\%the activation energy of NTQ=5 as physically close
\%the activation energy of TQ=20 as physically close
guessparams2=[1,5,10,20];

\%\% Plotting Data and guessparameters

figure(1)
plot(x,y,'xb',xx,NTQ_m1_w1_fixedIO(guessparams1,xx,IO1),'--r',xx,NTQ_m1_w1_fixedIO(guessparams1,xx,IO2),'--k',xx,NTQ_m1_w1_fixedIO(guessparams1,xx,IO3),
'--b',xx,NTQ_m1_w1_fixedIO(guessparams1,xx,IO4),'--m',xx,NTQ_m1_w1_fixedIO(guessparams1,xx,IO5),'--c',xx,
NTQ_m1_w1_fixedIO(guessparams1,xx,IO6),'-.r',xx,NTQ_m1_w1_fixedIO(guessparams1,xx,IO7),'-.k',xx,NTQ_m1_w1_fixedIO(guessparams1,xx,IO8),
'-.b',xx,NTQ_m1_w1_fixedIO(guessparams1,xx,IO9),'-.m',xx,NTQ_m1_w1_fixedIO(guessparams1,xx,IO10),'-.c')
xlabel('1/Temperature (1/K)')
ylabel('Intensity (a.u.)')
title('Experimental data and guess parameters1')
axis tight
v = axis;
axis([v(1),v(2),(v(3)*0.9),(v(4)*1.1)])
legend('Experimental Data','10\%','20\%','30\%','40\%','50\%','60\%','70\%','80\%','90\%','100\%','Location','NorthEastOutside')

figure(2)
plot(x,y,'xb',xx,NTQ_m1_w1_fixedIO(guessparams2,xx,IO1),'--r',xx,NTQ_m1_w1_fixedIO(guessparams2,xx,IO2),'--k',xx,NTQ_m1_w1_fixedIO(guessparams2,xx,IO3),
'--b',xx,NTQ_m1_w1_fixedIO(guessparams2,xx,IO4),'--m',xx,NTQ_m1_w1_fixedIO(guessparams2,xx,IO5),'--c',xx,
NTQ_m1_w1_fixedIO(guessparams2,xx,IO6),'-.r',xx,NTQ_m1_w1_fixedIO(guessparams2,xx,IO7),'-.k',xx,NTQ_m1_w1_fixedIO(guessparams2,xx,IO8),
'-.b',xx,NTQ_m1_w1_fixedIO(guessparams2,xx,IO9),'-.m',xx,NTQ_m1_w1_fixedIO(guessparams2,xx,IO10),'-.c')
xlabel('1/Temperature (1/K)')
ylabel('Intensity (a.u.)')
title('Experimental data and guess parameters2')
axis tight
v = axis;
axis([v(1),v(2),(v(3)*0.9),(v(4)*1.1)])
legend('Experimental Data','10\%','20\%','30\%','40\%','50\%','60\%','70\%','80\%','90\%','100\%','Location','NorthEastOutside')

\%\% Using fminsearch to find better parameters
```

```
options = optimset('MaxFunEvals',100000,'MaxIter',100000);
[IO1P1,chi1p1] = fminsearch('chi_no_sigma_fixedIO1',guessparams1,options);
[IO2P1,chi2p1] = fminsearch('chi_no_sigma_fixedIO2',guessparams1,options);
[IO3P1,chi3p1] = fminsearch('chi_no_sigma_fixedIO3',guessparams1,options);
[IO4P1,chi4p1] = fminsearch('chi_no_sigma_fixedIO4',guessparams1,options);
[IO5P1,chi5p1] = fminsearch('chi_no_sigma_fixedIO5',guessparams1,options);
[IO6P1,chi6p1] = fminsearch('chi_no_sigma_fixedIO6',guessparams1,options);
[IO7P1,chi7p1] = fminsearch('chi_no_sigma_fixedIO7',guessparams1,options);
[IO8P1,chi8p1] = fminsearch('chi_no_sigma_fixedIO8',guessparams1,options);
[IO9P1,chi9p1] = fminsearch('chi_no_sigma_fixedIO9',guessparams1,options);
[IO10P1,chi10p1] = fminsearch('chi_no_sigma_fixedIO10',guessparams1,options);
[IO1P2,chi1p2] = fminsearch('chi_no_sigma_fixedIO1',guessparams2,options);
[IO2P2,chi2p2] = fminsearch('chi_no_sigma_fixedIO2',guessparams2,options);
[IO3P2,chi3p2] = fminsearch('chi_no_sigma_fixedIO3',guessparams2,options);
[IO4P2,chi4p2] = fminsearch('chi_no_sigma_fixedIO4',guessparams2,options);
[IO5P2,chi5p2] = fminsearch('chi_no_sigma_fixedIO5',guessparams2,options);
[IO6P2,chi6p2] = fminsearch('chi_no_sigma_fixedIO6',guessparams2,options);
[IO7P2,chi7p2] = fminsearch('chi_no_sigma_fixedIO7',guessparams2,options);
[IO8P2,chi8p2] = fminsearch('chi_no_sigma_fixedIO8',guessparams2,options);
[IO9P2,chi9p2] = fminsearch('chi_no_sigma_fixedIO9',guessparams2,options);
[IO10P2,chi10p2] = fminsearch('chi_no_sigma_fixedIO10',guessparams2,options);

figure(3)
plot(x,y,'xb',xx,NTQ_m1_w1_fixedIO(IO1P1,xx,IO1),'--r',xx,NTQ_m1_w1_fixedIO(IO2P1,xx,IO2),'--k',xx,NTQ_m1_w1_fixedIO(IO3P1,xx,IO3),
'--b',xx,NTQ_m1_w1_fixedIO(IO4P1,xx,IO4),'--m',xx,NTQ_m1_w1_fixedIO(IO5P1,xx,IO5),'--c',xx,
NTQ_m1_w1_fixedIO(IO6P1,xx,IO6),'-.r',xx,NTQ_m1_w1_fixedIO(IO7P1,xx,IO7),'-.k',xx,NTQ_m1_w1_fixedIO(IO8P1,xx,IO8),
'-.b',xx,NTQ_m1_w1_fixedIO(IO9P1,xx,IO9),'-.m',xx,NTQ_m1_w1_fixedIO(IO10P1,xx,IO10),'-.c')
xlabel('1/Temperature (1/K)')
ylabel('Intensity (a.u.)')
title('Experimental data and P1')
axis tight
v = axis;
axis([v(1),v(2),(v(3)*0.9),(v(4)*1.1)])
legend('Experimental Data','10\%','20\%','30\%','40\%','50\%','60\%','70\%','80\%','90\%','100\%','Location','NorthEastOutside')

figure(4)
plot(x,y,'xb',xx,NTQ_m1_w1_fixedIO(IO1P2,xx,IO1),'--r',xx,NTQ_m1_w1_fixedIO(IO2P2,xx,IO2),'--k',xx,NTQ_m1_w1_fixedIO(IO3P2,xx,IO3),
'--b',xx,NTQ_m1_w1_fixedIO(IO4P2,xx,IO4),'--m',xx,NTQ_m1_w1_fixedIO(IO5P2,xx,IO5),'--c',xx,
NTQ_m1_w1_fixedIO(IO6P2,xx,IO6),'-.r',xx,NTQ_m1_w1_fixedIO(IO7P2,xx,IO7),'-.k',xx,NTQ_m1_w1_fixedIO(IO8P2,xx,IO8),
'-.b',xx,NTQ_m1_w1_fixedIO(IO9P2,xx,IO9),'-.m',xx,NTQ_m1_w1_fixedIO(IO10P2,xx,IO10),'-.c')
xlabel('1/Temperature (1/K)')
ylabel('Intensity (a.u.)')
title('Experimental data and P2')
axis tight
v = axis;
axis([v(1),v(2),(v(3)*0.9),(v(4)*1.1)])
legend('Experimental Data','10\%','20\%','30\%','40\%','50\%','60\%','70\%','80\%','90\%','100\%','Location','NorthEastOutside')


\%\% Comparing parameter shift

xpercent=[10,20,30,40,50,60,70,80,90,100];
D1P1=[IO1P1(1),IO2P1(1),IO3P1(1),IO4P1(1),IO5P1(1),IO6P1(1),IO7P1(1),IO8P1(1),IO9P1(1),IO10P1(1)];
E1P1=[IO1P1(2),IO2P1(2),IO3P1(2),IO4P1(2),IO5P1(2),IO6P1(2),IO7P1(2),IO8P1(2),IO9P1(2),IO10P1(2)];
C1P1=[IO1P1(3),IO2P1(3),IO3P1(3),IO4P1(3),IO5P1(3),IO6P1(3),IO7P1(3),IO8P1(3),IO9P1(3),IO10P1(3)];
E2P1=[IO1P1(4),IO2P1(4),IO3P1(4),IO4P1(4),IO5P1(4),IO6P1(4),IO7P1(4),IO8P1(4),IO9P1(4),IO10P1(4)];
D1P2=[IO1P2(1),IO2P2(1),IO3P2(1),IO4P2(1),IO5P2(1),IO6P2(1),IO7P2(1),IO8P2(1),IO9P2(1),IO10P2(1)];
E1P2=[IO1P2(2),IO2P2(2),IO3P2(2),IO4P2(2),IO5P2(2),IO6P2(2),IO7P2(2),IO8P2(2),IO9P2(2),IO10P2(2)];
C1P2=[IO1P2(3),IO2P2(3),IO3P2(3),IO4P2(3),IO5P2(3),IO6P2(3),IO7P2(3),IO8P2(3),IO9P2(3),IO10P2(3)];
E2P2=[IO1P2(4),IO2P2(4),IO3P2(4),IO4P2(4),IO5P2(4),IO6P2(4),IO7P2(4),IO8P2(4),IO9P2(4),IO10P2(4)];
```

```
figure(5)
plot(xpercent,D1P1,'--r',xpercent,E1P1,'--b',xpercent,C1P1,'--m',xpercent,E2P1,'--k',xpercent,D1P2,'-.r',xpercent,E1P2,'-.b',xpercent,C1P2,
'-.m',xpercent,E2P2,'-.k')
xlabel('Percentage of minimum intensity giving fixed Io')
ylabel('a.u')
title('Exploring Io paramter space')
axis tight
v = axis;
axis([v(1),v(2),(v(3)*0.9),(v(4)*1.1)])
legend('D1P1','E1P1','C1P1','E2P1','D1P2','E1P2','C1P2','E2P2','Location','NorthEastOutside')

if (IO1P1-IO1P2)<=[0.001,0.001,0.001,0.001]
    AIO1=(IO1P1+IO1P2)./2;
else
    if abs(chi1p1)<abs(chi1p2)
        AIO1=IO1P1;
    else
        AIO1=IO1P2;
    end
    display('10\% didnt agree')
end
if (IO2P1-IO2P2)<=[0.001,0.001,0.001,0.001]
    AIO2=(IO2P1+IO2P2)./2;
else
    if abs(chi2p1)<abs(chi2p2)
        AIO2=IO2P1;
    else
        AIO2=IO2P2;
    end
    display('20\% didnt agree')
end
if (IO3P1-IO3P2)<=[0.001,0.001,0.001,0.001]
    AIO3=(IO3P1+IO3P2)./2;
else
    if abs(chi3p1)<abs(chi3p2)
        AIO3=IO3P1;
    else
        AIO3=IO3P2;
    end
    display('30\% didnt agree')
end
if (IO4P1-IO4P2)<=[0.001,0.001,0.001,0.001]
    AIO4=(IO4P1+IO4P2)./2;
else
    if abs(chi4p1)<abs(chi4p2)
        AIO4=IO4P1;
    else
        AIO4=IO4P2;
    end
    display('40\% didnt agree')
end
if (IO5P1-IO5P2)<=[0.001,0.001,0.001,0.001]
    AIO5=(IO5P1+IO5P2)./2;
else
    if abs(chi5p1)<abs(chi5p2)
        AIO5=IO5P1;
    else
        AIO5=IO5P2;
    end
```

```
    display('50\% didnt agree')
end
if (IO6P1-IO6P2)<=[0.001,0.001,0.001,0.001]
    AIO6=(IO6P1+IO6P2)./2;
else
    if abs(chi6p1)<abs(chi6p2)
        AIO6=IO6P1;
    else
        AIO6=IO6P2;
    end
    display('60\% didnt agree')
end
if (IO7P1-IO7P2)<=[0.001,0.001,0.001,0.001]
    AIO7=(IO7P1+IO7P2)./2;
else
    if abs(chi7p1)<abs(chi7p2)
        AIO7=IO7P1;
    else
        AIO7=IO7P2;
    end
    display('70\% didnt agree')
end
if (IO8P1-IO8P2)<=[0.001,0.001,0.001,0.001]
    AIO8=(IO8P1+IO8P2)./2;
else
    if abs(chi8p1)<abs(chi8p2)
        AIO8=IO8P1;
    else
        AIO8=IO8P2;
    end
    display('80\% didnt agree')
end
if (IO9P1-IO9P2)<=[0.001,0.001,0.001,0.001]
    AIO9=(IO9P1+IO9P2)./2;
else
    if abs(chi9p1)<abs(chi9p2)
        AIO9=IO9P1;
    else
        AIO9=IO9P2;
    end
    display('90\% didnt agree')
end
if (IO10P1-IO10P2)<=[0.001,0.001,0.001,0.001]
    AIO10=(IO10P1+IO10P2)./2;
else
    if abs(chi10p1)<abs(chi10p2)
        AIO10=IO10P1;
    else
        AIO10=IO10P2;
    end
    display('100\% didnt agree')
end


xpercent=[10,20,30,40,50,60,70,80,90,100];
D1=[AIO1(1),AIO2(1),AIO3(1),AIO4(1),AIO5(1),AIO6(1),AIO7(1),AIO8(1),AIO9(1),AIO10(1)]
E1=[AIO1(2),AIO2(2),AIO3(2),AIO4(2),AIO5(2),AIO6(2),AIO7(2),AIO8(2),AIO9(2),AIO10(2)]
C1=[AIO1(3),AIO2(3),AIO3(3),AIO4(3),AIO5(3),AIO6(3),AIO7(3),AIO8(3),AIO9(3),AIO10(3)]
E2=[AIO1(4),AIO2(4),AIO3(4),AIO4(4),AIO5(4),AIO6(4),AIO7(4),AIO8(4),AIO9(4),AIO10(4)]
```

```
figure(6)
plot(xpercent,D1,'--r',xpercent,E1,'--b',xpercent,C1,'--m',xpercent,E2,'--k')
xlabel('Percentage of minimum intensity giving fixed Io')
ylabel('a.u')
title('Exploring Io paramter space')
axis tight
v = axis;
axis([v(1),v(2),(v(3)*0.9),(v(4)*1.1)])
legend('D1','E1','C1','E2','Location','NorthEastOutside')


display('Type in A# for the percent that it last fails on, A0 if it works')
display('Io, +-, D1, +-, E1, +-, C1, +-, E2, +-')

    \%calculating average without 10\%, 20\%, 30\%, 40\%, 50\%, 60\%, 70\%, 80\%
    A80(1)=sum([IO9,IO10])/2;
    A80(2)=range([IO9,IO10])/2;
    A80(3)=sum([AIO9(1),AIO10(1)])/2;
    A80(4)=range([AIO9(1),AIO10(1)])/2;
    A80(5)=sum([AIO9(2),AIO10(2)])/2;
    A80(6)=range([AIO9(2),AIO10(2)])/2;
    A80(7)=sum([AIO9(3),AIO10(3)])/2;
    A80(8)=range([AIO9(3),AIO10(3)])/2;
    A80(9)=sum([AIO9(4),AIO10(4)])/2;
    A80(10)=range([AIO9(4),AIO10(4)])/2;
    \%calculating average without 10\%, 20\%, 30\%, 40\%, 50\%, 60\%, 70\%
    A70(1)=sum([IO8,IO9,IO10])/3;
    A70(2)=range([IO8,IO9,IO10])/2;
    A70(3)=sum([AIO8(1),AIO9(1),AIO10(1)])/3;
    A70(4)=range([AIO8(1),AIO9(1),AIO10(1)])/2;
    A70(5)=sum([AIO8(2),AIO9(2),AIO10(2)])/3;
    A70(6)=range([AIO8(2),AIO9(2),AIO10(2)])/2;
    A70(7)=sum([AIO8(3),AIO9(3),AIO10(3)])/3;
    A70(8)=range([AIO8(3),AIO9(3),AIO10(3)])/2;
    A70(9)=sum([AIO8(4),AIO9(4),AIO10(4)])/3;
    A70(10)=range([AIO8(4),AIO9(4),AIO10(4)])/2;
    \%calculating average without 10\%, 20\%, 30\%, 40\%, 50\%, 60\%
    A60(1)=sum([IO7,IO8,IO9,IO10])/4;
    A60(2)=range([IO7,IO8,IO9,IO10])/2;
    A60(3)=sum([AIO7(1),AIO8(1),AIO9(1),AIO10(1)])/4;
    A60(4)=range([AIO7(1),AIO8(1),AIO9(1),AIO10(1)])/2;
    A60(5)=sum([AIO7(2),AIO8(2),AIO9(2),AIO10(2)])/4;
    A60(6)=range([AIO7(2),AIO8(2),AIO9(2),AIO10(2)])/2;
    A60(7)=sum([AIO7(3),AIO8(3),AIO9(3),AIO10(3)])/4;
    A60(8)=range([AIO7(3),AIO8(3),AIO9(3),AIO10(3)])/2;
    A60(9)=sum([AIO7(4),AIO8(4),AIO9(4),AIO10(4)])/4;
    A60(10)=range([AIO7(4),AIO8(4),AIO9(4),AIO10(4)])/2;
    \%calculating average without 10\%, 20\%, 30\%, 40\%, 50\%
    A50(1)=sum([IO6,IO7,IO8,IO9,IO10])/5;
    A50(2)=range([IO6,IO7,IO8,IO9,IO10])/2;
    A50(3)=sum([AIO6(1),AIO7(1),AIO8(1),AIO9(1),AIO10(1)])/5;
    A50(4)=range([AIO6(1),AIO7(1),AIO8(1),AIO9(1),AIO10(1)])/2;
    A50(5)=sum([AIO6(2),AIO7(2),AIO8(2),AIO9(2),AIO10(2)])/5;
    A50(6)=range([AIO6(2),AIO7(2),AIO8(2),AIO9(2),AIO10(2)])/2;
    A50(7)=sum([AIO6(3),AIO7(3),AIO8(3),AIO9(3),AIO10(3)])/5;
    A50(8)=range([AIO6(3),AIO7(3),AIO8(3),AIO9(3),AIO10(3)])/2;
    A50(9)=sum([AIO6(4),AIO7(4),AIO8(4),AIO9(4),AIO10(4)])/5;
    A50(10)=range([AIO6(4),AIO7(4),AIO8(4),AIO9(4),AIO10(4)])/2;
    \%calculating average without 10\%, 20\%, 30\%, 40\%
    A40(1)=sum([IO5,IO6,IO7,IO8,IO9,IO10])/6;
```

```
    A40(2)=range([IO5,IO6,IO7,IO8,IO9,IO10])/2;
    A40(3)=sum([AIO5(1),AIO6(1),AIO7(1),AIO8(1),AIO9(1),AIO10(1)])/6;
    A40(4)=range([AIO5(1),AIO6(1),AIO7(1),AIO8(1),AIO9(1),AIO10(1)])/2;
    A40(5)=sum([AIO5(2),AIO6(2),AIO7(2),AIO8(2),AIO9(2),AIO10(2)])/6;
    A40(6)=range([AIO5(2),AIO6(2),AIO7(2),AIO8(2),AIO9(2),AIO10(2)])/2;
    A40(7)=sum([AIO5(3),AIO6(3),AIO7(3),AIO8(3),AIO9(3),AIO10(3)])/6;
    A40(8)=range([AIO5(3),AIO6(3),AIO7(3),AIO8(3),AIO9(3),AIO10(3)])/2;
    A40(9)=sum([AIO5(4),AIO6(4),AIO7(4),AIO8(4),AIO9(4),AIO10(4)])/6;
    A40(10)=range([AIO5(4),AIO6(4),AIO7(4),AIO8(4),AIO9(4),AIO10(4)])/2;
    \%calculating average without 10\%, 20\%, 30\%
    A30(1)=sum([IO4,IO5,IO6,IO7,IO8,IO9,IO10])/7;
    A30(2)=range([IO4,IO5,IO6,IO7,IO8,IO9,IO10])/2;
    A30(3)=sum([AIO4(1),AIO5(1),AIO6(1),AIO7(1),AIO8(1),AIO9(1),AIO10(1)])/7;
    A30(4)=range([AIO4(1),AIO5(1),AIO6(1),AIO7(1),AIO8(1),AIO9(1),AIO10(1)])/2;
    A30(5)=sum([AIO4(2),AIO5(2),AIO6(2),AIO7(2),AIO8(2),AIO9(2),AIO10(2)])/7;
    A30(6)=range([AIO4(2),AIO5(2),AIO6(2),AIO7(2),AIO8(2),AIO9(2),AIO10(2)])/2;
    A30(7)=sum([AIO4(3),AIO5(3),AIO6(3),AIO7(3),AIO8(3),AIO9(3),AIO10(3)])/7;
    A30(8)=range([AIO4(3),AIO5(3),AIO6(3),AIO7(3),AIO8(3),AIO9(3),AIO10(3)])/2;
    A30(9)=sum([AIO4(4),AIO5(4),AIO6(4),AIO7(4),AIO8(4),AIO9(4),AIO10(4)])/7;
    A30(10)=range([AIO4(4),AIO5(4),AIO6(4),AIO7(4),AIO8(4),AIO9(4),AIO10(4)])/2;
    \%calculating average without 10\%, 20\%
    A20(1)=sum([IO3,IO4,IO5,IO6,IO7,IO8,IO9,IO10])/8;
    A20(2)=range([IO3,IO4,IO5,IO6,IO7,IO8,IO9,IO10])/2;
    A20(3)=sum([AIO3(1),AIO4(1),AIO5(1),AIO6(1),AIO7(1),AIO8(1),AIO9(1),AIO10(1)])/8;
    A20(4)=range([AIO3(1),AIO4(1),AIO5(1),AIO6(1),AIO7(1),AIO8(1),AIO9(1),AIO10(1)])/2;
    A20(5)=sum([AIO3(2),AIO4(2),AIO5(2),AIO6(2),AIO7(2),AIO8(2),AIO9(2),AIO10(2)])/8;
    A20(6)=range([AIO3(2),AIO4(2),AIO5(2),AIO6(2),AIO7(2),AIO8(2),AIO9(2),AIO10(2)])/2;
    A20(7)=sum([AIO3(3),AIO4(3),AIO5(3),AIO6(3),AIO7(3),AIO8(3),AIO9(3),AIO10(3)])/8;
    A20(8)=range([AIO3(3),AIO4(3),AIO5(3),AIO6(3),AIO7(3),AIO8(3),AIO9(3),AIO10(3)])/2;
    A20(9)=sum([AIO3(4),AIO4(4),AIO5(4),AIO6(4),AIO7(4),AIO8(4),AIO9(4),AIO10(4)])/8;
    A20(10)=range([AIO3(4),AIO4(4),AIO5(4),AIO6(4),AIO7(4),AIO8(4),AIO9(4),AIO10(4)])/2;
    \%calculating average without 10\%
    A10(1)=sum([IO2,IO3,IO4,IO5,IO6,IO7,IO8,IO9,IO10])/9;
    A10(2)=range([IO2,IO3,IO4,IO5,IO6,IO7,IO8,IO9,IO10])/2;
    A10(3)=sum([AIO2(1),AIO3(1),AIO4(1),AIO5(1),AIO6(1),AIO7(1),AIO8(1),AIO9(1),AIO10(1)])/9;
    A10(4)=range([AIO2(1),AIO3(1),AIO4(1),AIO5(1),AIO6(1),AIO7(1),AIO8(1),AIO9(1),AIO10(1)])/2;
    A10(5)=sum([AIO2(2),AIO3(2),AIO4(2),AIO5(2),AIO6(2),AIO7(2),AIO8(2),AIO9(2),AIO10(2)])/9;
    A10(6)=range([AIO2(2),AIO3(2),AIO4(2),AIO5(2),AIO6(2),AIO7(2),AIO8(2),AIO9(2),AIO10(2)])/2;
    A10(7)=sum([AIO2(3),AIO3(3),AIO4(3),AIO5(3),AIO6(3),AIO7(3),AIO8(3),AIO9(3),AIO10(3)])/9;
    A10(8)=range([AIO2(3),AIO3(3),AIO4(3),AIO5(3),AIO6(3),AIO7(3),AIO8(3),AIO9(3),AIO10(3)])/2;
    A10(9)=sum([AIO2(4),AIO3(4),AIO4(4),AIO5(4),AIO6(4),AIO7(4),AIO8(4),AIO9(4),AIO10(4)])/9;
    A10(10)=range([AIO2(4),AIO3(4),AIO4(4),AIO5(4),AIO6(4),AIO7(4),AIO8(4),AIO9(4),AIO10(4)])/2;
    \%calculating average
    A0(1)=sum([IO1,IO2,IO3,IO4,IO5,IO6,IO7,IO8,IO9,IO10])/10;
    A0(2)=range([IO1,IO2,IO3,IO4,IO5,IO6,IO7,IO8,IO9,IO10])/2;
    A0(3)=sum([AIO1(1),AIO2(1),AIO3(1),AIO4(1),AIO5(1),AIO6(1),AIO7(1),AIO8(1),AIO9(1),AIO10(1)])/10;
    A0(4)=range([AIO1(1),AIO2(1),AIO3(1),AIO4(1),AIO5(1),AIO6(1),AIO7(1),AIO8(1),AIO9(1),AIO10(1)])/2;
    A0(5)=sum([AIO1(2),AIO2(2),AIO3(2),AIO4(2),AIO5(2),AIO6(2),AIO7(2),AIO8(2),AIO9(2),AIO10(2)])/10;
    A0(6)=range([AIO1(2),AIO2(2),AIO3(2),AIO4(2),AIO5(2),AIO6(2),AIO7(2),AIO8(2),AIO9(2),AIO10(2)])/2;
    A0(7)=sum([AIO1(3),AIO2(3),AIO3(3),AIO4(3),AIO5(3),AIO6(3),AIO7(3),AIO8(3),AIO9(3),AIO10(3)])/10;
    A0(8)=range([AIO1(3),AIO2(3),AIO3(3),AIO4(3),AIO5(3),AIO6(3),AIO7(3),AIO8(3),AIO9(3),AIO10(3)])/2;
    A0(9)=sum([AIO1(4),AIO2(4),AIO3(4),AIO4(4),AIO5(4),AIO6(4),AIO7(4),AIO8(4),AIO9(4),AIO10(4)])/10;
    A0(10)=range([AIO1(4),AIO2(4),AIO3(4),AIO4(4),AIO5(4),AIO6(4),AIO7(4),AIO8(4),AIO9(4),AIO10(4)])/2;
```

The function used to calculated the fitted values from parameters

```
function I = NTQ_m1_w1_fixedIO(parameters,x,IO)
\%\% function for Fitting negative thermal quenching m=1 w=1
```

```
kb =8.6173e-0002;
D1 = parameters(1);
E1 = parameters(2);
C1 = parameters(3);
E2 = parameters(4);

I=IO*((1+D1.*exp(-E1./(kb.*x))./(1+C1.*exp(-E2./(kb.*x))));
```

and the finally an example of function used to calculated the chi-squared as one is required for each I(0) value

```
function chi=chi_no_sigma_fixedIO1(parameters)
\% chi^2 function for Fitting negative thermal quenching m=1 w=1
\% with no known error

global x y IO1
chi= sum(((y-NTQ_m1_w1_fixedIO(parameters,x,IO1)).^2)./NTQ_m1_w1_fixedIO(parameters,x,IO1));
```

7.2 Appendix II

The piece of code used to calculated the rotational and vibrational excited states of the neutral donor bound excitons:

```
\%\% Calculating vibration and rotational states of bound excitons
\% using the function
\% E(nu,J)=-(2*m*a^2*L^2/hbar^2)/((nu+1/2)+sqrt((J+1/2)^2+(2*m*a^2*L/hbar^2)))^2
\% for ZnO m=0.7mo and a=0.8nm
\% version 1 (20/01/2013)
\%
\%\% Clearing old data
clc
clear all

\%\% Getting user input of the localisation energy

L = input('input the localisation energy in meV = ');

\%\% pre allocating and defining constants
x = 19.1-L;
L=L/1000*(1.60217657*10^(-19)); \%J
m = 0.7*9.10938215*10^(-31); \%kg
a = 0.8*10^(-9); \%m
hbar = 1.05457173*10^(-34); \%Kg m^2 s or J s^-1
E = zeros(4,4);
A = (2*m*a^2*L^2/hbar^2);
B = A/L;

\%\% Calculating the energy shift

for nu=1:3
    for J=1:3
        E(nu,J)=-(A)/((nu-1+1/2)+sqrt((J-1+1/2)^2+B))^2;
    end
end

E = E*(6.24150932*10^18)*1000; \%meV
```

```
C = -E(1,1);
E(1,1) = 0;
E = E+C;
display('E(0,0) and energy above ground state (meV)')
E
display('Energy of states (eV)')
Z=E;
Z(1,1)=0;
Z./1000+3.3567+x/1000
```

Chapter 8

Acknowledgements

First of all I would like to thank my supervisors Martin Allen and Roger Reeves. Roger Reeves for his all encompassing knowledge in the lab and his seemingly unending patience when making corrections on my thesis. Martin Allen for his constant ability to think up experiments and explain the possible nature of features. I would like to acknowledge the support of the amazing technical staff who supplied me with liquid He and help with troubleshooting lab equipment. In particular I would like to thank Stephen Hemmingsen as he bore the brunt of my issues. Without the help of Robert Heinhold and Konstantin Ivanovskikh my experimental ability will be severely crippled as their expertise was constantly available.

I would also like to thank my colleagues Rosa Hughes-Currie, Chrissy Emeny, Alex Salkeld, Ian Farrell, Mohammad Zeidan, Sophie Koster, Pubudu Senanayake and many more for their distractions, discussion and help throughout this experience.

Bibliography

[1] Maeda K, Sato M, Niikura I, and Fukuda T. *Growth of* 2 *inch ZnO bulk single crystal by the hydrothermal method.* Semiconductor Science and Technology, 20:S49–S54, (2005).

[2] Heinhold R. *PhD Thesis awaiting submission.* University of Canterbury, (2014).

[3] Niguera C. *Polar oxide surfaces.* Journal of Physics: Condensed Matter, 12:R367–R410, (2000).

[4] Heinhold R and Allen M W. *Polarity-denpendent photoemission of in situ cleaved zinc oxide single crystals.* Journal of Materials Research, 27:2214–2219, (2012).

[5] Coskun C, Look D C, Farlow G C, and Sizelove J R. *Radiation hardness of ZnO at low temperatures.* Semiconductor Science and Technology, 19:752–754, (2004).

[6] Tuomisto F, Look D C, and Farlow G C. *Defect studies in electron-irradiated ZnO and GaN.* Physica B: Condensed Matter, 401:604–608, (2007).

[7] Kennedy J, Carder D A, Markwitz A, and Reeves R J. *Properties of nitrogen implanted and electron beam annealed bulk ZnO.* Journal of Applied Physics, 107:103518, (2010).

[8] High A A, Novitskaya E E, Butov L V, Hanson M, and Gossard A C. *Control of exciton fluxes in an excitonic integrated circuit.* Science, 321:229–231, (2008).

[9] Heiland G, Mollwo E, and Stockmann F. *Electronic processes in Zinc Oxide.* Solid State Physics, Advances in research and applications, 8:191, (1959).

[10] Look D C, Hemsky J W, and Sizelove J R. *Residual Native Shallow Donor in ZnO.* Physical Review Letters, 82:2552–2555, (1999).

[11] Van de Walle C G. *Hydrogen as a cause of doping in Zinc Oxide.* Physical Review Letters, 85:1012–1015, (2000).

[12] Meyer B K, Alves H, Hofmann D M, Kriegseis W, Forster D, Bertram F, Christen J, Hoffmann A, Straburg M, Dworzak M, Haboeck U, and Rodina A V. *Bound exciton and donoracceptor pair recombinations in ZnO.* Physica Status Solidi (b), 241:231–260, (2004).

[13] Van de Walle C G and Neugebauer J. *Hydrogen in Semiconductors.* Annual Review of Material Research, 36:179–198, (2006).

[14] Hofmann D M, Hofstaetter A, Leiter F, Zhou H, Henecker F, Meyer B K, Orlinskii S B, Schmidt J, and Baranov P G. *Hydrogen: A relevant shallow donor in zinc oxide.* Physical Review Letters, 88:045504, (2002).

[15] McCluskey M D, Tarun M C, and Teklemichael S T. *Hydrogen in oxide semiconductors.* Journal of Materials Research, 27:2190–2198, (2012).

[16] Matsubara M, Amini M N, Saniz R, Lamoen D, and Partoens B. *Attracting shallow donors: Hydrogen passivation in (Al,Ga,In)-doped ZnO.* Physics Review B, 86:165207, (2012).

[17] Shin J W, No Y S, Lee J Y, Choi W K, and Kim T W. *Effects of different annealing atmospheres on the surface and microstructural properties of ZnO thin films grown on p-Si* (100) *substrates.* Applied Surface Science, 257:7516–7520, (2011).

[18] Dangbégnon J K, Talla K, and Botha J R. *Effect of the annealing environment on the optical properties of ZnO/GaAs grown by MOCVD.* Journal of Luminescence, 131:2457–2462, (2011).

[19] Shibata H. *Negative thermal quenching curves in photoluminescence of solids.* Japanese Journal of Applied Physics, 37:550–553, (1998).

[20] Denisov M M and Makarov V P. *Longitudinal and Transverse Excitons in Semiconductors.* Physica Status Solidi (*b*), 56:9–59, (1973).

[21] Zhang X B, Taliercio T, Kolliakos S, and Lefebvre P. *Influence of electron-phonon interaction on the optical properties of III nitride semiconductors.* Journal of Physics: Condensed Matter, 13:7053–7074, (2001).

[22] Meyer B K, Sann J, Lautenschlager S, Wagner M R, and Hoffmann A. *Ionized and neutral donor-bound excitons in ZnO.* Physical Review B, 72:184120, (2007).

[23] Wagner M R, Callsen G, Reparaz J S, Schulze J H, Kirste R, Cobet M, Ostapenko I A, Rodt S, Nenstiel C, Kaiser M, Hoffmann A, Rodina A V, Phillips M R, Lautenschlager S, Eisermann S, and Meyer B K. *Bound excitons in ZnO : structural defect complexes versus shallow impurity centers.* Physical Review B, 84:035313, (2011).

[24] Meyer B K, Sann J, Eisermann S, Lautenschlaeger S, Wagner M R, Kaiser M, Callsen G, Reparaz J S, and Hoffmann A. *Excited state properties of donor bound excitons in ZnO.* Physical Review B, 82:115207, (2010).

[25] Bayrak O, Boztosun I, and Ciftci H. *Exact analytical solutions to the Kratzer potential by the asymptotic interation method.* International Journal of Quantum Chemistry, 107:540–544, (2007).

[26] Heinhold R, Kim H S, Schmidt F, von Wenckstern H, Grundmann M, Mendelsberg R J, Reeves R J, Durbin S M, and Allen M W. *Optical and defect properties*

of hydrothermal ZnO with low lithium contamination. Applied Physics Letters, 101:062105, (2012).

[27] M Lynam. *PhD Thesis awaiting submission.* University of Canterbury, (2015).

[28] Dong Y, Fang Z-Q, Look D C, Cantwell G, Zhang J, Song J J, and Brillson L J. *Zn- and O-face polarity effects at ZnO surfaces and metal interfaces.* Applied Physics Letters, 93:072111, (2008).

[29] Garces N Y, Wang L, Bai L, Giles N C, Halliburton L E, and Cantwell G. *Role of copper in the green luminescence from ZnO crystals.* Journal of Materials Research, 81:622, (2002).

[30] Mendelsberg R. *Photoluminescence of ZnO grown by eclipse pulsed laser deposition.* University of Canterbury, PhD thesis, (2009).